Fuente Herraiz, D.; Lazar, D.; Oliver Villanueva, JV.; Urchueguía Schölzel, JF. (2021). Reconstruction of the absorption spectrum of Synechocystis sp. PCC 6803 optical mutants from the in vivo signature of individual pigments. Photosynthesis Research. 147(1):75-90. https://doi.org/10.1007/s11120-020-00799-8

Reconstruction of the absorption spectrum of *Synechocystis* sp. PCC 6803 optical mutants from the in vivo signature of individual pigments

David Fuente*, Dušan Lazár, Jose Vicente Oliver-Villanueva, and Javier F. Urchueguía

Instituto de Aplicaciones de las Tecnologías de la Información y de las Comunicaciones Avanzadas, Universitat Politècnica de València, Valencia, Spain (D.F., J.V.O.-V., J.F.U.)

Department of Biophysics, Faculty of Science, Palacký University, Olomouc, Czech Republic (D.F., D.L.)

Department of Adaptation Biotechnologies, Global Change Research Centre, Academy of Science of the Czech Republic, Drásov, Czech Republic (D.F.)

*Corresponding author: dafueher@upv.es

ORCID IDs: 0000-0003-4141-7948 (D.F.); 0000-0001-8035-4017 (D.L.); 0000-0003-2842-7834 (J.V.O.-V.); 0000-0001-7618-8204 (J.F.U.)

D.F. and J.F.U. conceived the research; D.F. did the experiments; D.F. and J.V.O.-V. performed the simulations; D.F., D.L. and J.F.U. analyzed the data; D.F. wrote the manuscript with contributions from D.L., J.V.O.-V. and J.F.U. D.F. agrees to serve as the author responsible for contact and ensures communication.

D.F. was supported by an internal grant of Palacký University Olomouc (no. IGA_PrF_2020_028) and D.L. by the ERDF project “Plants as a tool for sustainable global development” (no. CZ.02.1.01/0.0/0.0/16-019/0000827)."

Abstract

In this work, we reconstructed the absorption spectrum of different *Synechocystis* sp. PCC 6803 optical strains by summing the computed signature of all pigments present in this organism. To do so, modifications to in vitro pigment spectra were first required: namely wavelength shift, curve smoothing and the package-effect calculation derived from high-pigment densities were applied. As a result, we outlined a plausible shape for the in vivo absorption spectrum of each chromophore. These are flatter and slightly broader in physiological conditions yet the mean weight-specific absorption coefficient remains identical to the in vitro conditions. Moreover, we give an estimate of all pigment concentrations without applying spectrophotometric correlations, which are often prone to error.

The computed cell spectrum reproduces in an accurate manner the experimental spectrum for all the studied wavelengths in the wild-type, Olive and PAL strain. The gathered pigment concentrations are in agreement with reported values in literature. Moreover, different illumination set-ups were evaluated to calculate the mean absorption cross-section of each chromophore. Finally, a qualitative estimate of light-limited cellular growth at each wavelength is given. This investigation describes a novel way to approach the cell absorption spectrum and shows all its inherent potential for photosynthesis research.

Keywords: absorption, spectrum, light, pigment, modeling, *Synechocystis*, photosystem

1 Introduction

1.1 Light spectrum influence in photosynthesis

Light is a principal factor regulating photosynthesis and influencing its global efficiency because light is the fundamental energy source for photosynthetic organisms and in many environments radiation is a limiting factor. The impact of light on the photosynthetic apparatus has been widely researched since the second half of last century and more recently in silico quantified (Westermark and Steuer 2016). An extensive variety of books and reviews on this matter (van Amerongen, van Grondelle, and Valkunas 2000; Green and Parson 2003) as well as on-line resources (Orr and Govindjee 2013) are available. Most of the published reference works on photosynthesis research treat light intensity as a scalar magnitude (Rabe and Benoit 1962) and neglect the effect of the photon flux distribution, while few recent works can be found assessing color effect experiments (Fuente et al. 2017; Manodori and Melis 1986; McGee et al. 2020; de Mooij et al. 2016; Münzner and Voigt 1992). Yet, it is well known that the photon flux distribution does not only affect photosynthetic processes in which only excitons are directly involved, but also different electron pathways (Ma et al. 2007) and consequently biomass formation as well. In this regard, many cyanobacterial strains such as the model organism *Synechocystis* sp. PCC 6803 (Knoop et al. 2010) (hereafter referred to as *Synechocystis*), present longer doubling times under pure blue light exposure (Singh et al. 2009) and in some cases even no experimental growth is appreciable and cultures collapse (Zavřel et al. 2015). On the contrary, orange-red radiation promotes in this strain much higher growth rates (Luimstra et al. 2018). Additionally, the wavelength effect is also perceptible on other photosynthesis processes in *Synechocystis* like non-photochemical quenching (NPQ), state transitions and chlorophyll fluorescence (Remelli and Santabarbara 2018; Stirbet et al. 2019; Zavřel, Očenášová, and Červený 2017). Identical situation regarding color influence on biomass creation occurs for *Arthrospira platensis*, which is a comparable species. However, in organisms owning other classes of pigments, like plants, different radiation wavelengths may support maximal productivities.

1.2 Absorption spectrum analysis and reconstruction

The analysis of absorption spectra is another technique that can throw light on the organism behavior. Indeed, it is quite common to measure the in vivo absorption signature to depict the cellular state under a wide range of experimental conditions such as light stress, nutrient deprivation or even for mutant-strain characterization. In particular, the exposure to high light (Kopečná et al. 2012) or different light types (Stramski and Morel 1990) modifies the cell absorption spectra due to variations in pigment composition and concentration. It is fundamental to correctly measure the cell absorption spectrum because scattering can mask real absorption if too dense cultures are employed or if the measurement is performed without an integrating sphere. This device practically, though not completely, eliminates the contribution of scattering to apparent absorption and thus, light harvesting might be overestimated without it. However, pigment absorption spectra cannot be directly measured in vivo and besides, organic solvents used for gathering in vitro properties can break down the pigment-protein complexes. As is well known, these interactions result in a band-shift towards longer wavelengths and a flattening of the absorption spectra with respect to in vitro conditions (Buschmann and Nagel 1993). For example, the cell-extract signature of a *Synechococcus* strain in an organic solvent presents several local minima-maxima in the blue-green band due to different carotenoid absorption peaks that are absent in the in vivo spectrum (Kilian et al. 2007). Moreover, polarity-induced changes within chromophores in high-polarizability solvents are due to an intramolecular-charge transfer state which can lead to spectrum broadening and interestingly, these solvents can mimic the electrostatic environment in physiological conditions (Gong et al. 2018). Nevertheless, absorption properties of chromophores under physiological conditions might differ just slightly from those in organic solvents as photo-acoustic methods suggest (Eng and Baranoski 2007; Herbert, Han, and Vogelmann 2000). Therefore, in vitro pigment signatures can serve for an approximate recreation of the cell absorption spectrum.

Previous investigations into pigment contribution to absorption can be found in literature, which basically follow two different strategies: either using pigment-solvent signatures (Bidigare et al. 1990; Bricaud et al. 2004) to construct the cell spectrum by summing them (Ficek et al. 2004; Fujiki and Taguchi 2002) or deconvolving the true in vivo absorption in different Gaussian curves (Hoepffner and Sathyendranath 1991; Thrane et al. 2015). The first approach is useful if the research wants to shed light on the spectral contribution of each pigment and their absorption spectra are known. The second can assess specific chromophore content at absorption peaks, but these Gaussian curves do not resemble actual pigment spectra and are a mere ad hoc method.

1.3 Pigment content estimation

Photoactive pigments are mostly located inside the plasma and thylakoid membranes in photosynthetic microorganisms but hyperspectral confocal fluorescence microscopy technique indicates that in cyanobacteria non-assembled phycobilin proteins can be found in the cytoplasm, too (Collins et al. 2012). On this subject, the calculation of each pigment concentration gives insight into the state of cells as the chromophores respond to stress and environmental changes, and are critical for a balanced light absorption. A common method for the assessment of the chlorophyll and carotenoid content is to extract them with organic solvents and quantify their amount by means of the HPLC technique. Alternatively, the measurement of the pigment content conforming the phycobilisomes is a challenging task. Traditional methods cannot extract such pigments using organic solvents due to their hydrophilic affinity. Additionally, the main phycobilins in *Synechocystis* cells, allophycocyanin and phycocyanin, display spectra that overlap the chlorophyll absorption spectrum, even in aqueous extracts due to cell disintegration. Thus, a precise estimation of the true in vivo absorption coefficients of the phycobilin pigments stacked in allophycocyanin (APC) and phycocyanin (PC) is rather complicated. Furthermore, phycobilin proteins are normally estimated in a spectrophotometric way by means of empirical equations that incorporate absorption measurements at specific wavelengths (Bennett and Bogobad 1973). However, even at these wavelengths the contribution of chlorophyll cannot be neglected since it can lead to inaccurate phycobilin quantification. Hence, protocols have to be updated to account with such pigment interference (Lauceri et al. 2018). In general, the application of wavelength equations is susceptible to imprecise pigment determination since it is an ad hoc method.

In summary, the quantification of cellular pigments via HPLC can be tedious and spectrophotometric correlations do not always deliver trustful results. Hence, it would be interesting to develop a formalism leveraging available physical and optical properties to gather approximate shapes of pigment absorption spectra. Those could be reused under different concentrations, growth conditions and even similar organisms. The creation of a library with in vivo pigment signatures could assist scientists in estimating the content of each light-harvesting compound and the absorbed photon-flux distribution under different light sources and organisms. We propose a methodology that updates prior reconstruction frameworks of the cell absorption spectrum: the chromophore spectra have to be previously shifted, packed but also smoothed. One of the most striking results of this work is the possibility of

reconstructing different strain spectra starting from the same in vivo pigment signatures, despite owning these strains dissimilar chromophore concentrations and pigment compositions. Their absorption signatures can be considered proportional to the chromophore concentration, thus estimated, and the absorbed photon-flux distribution also computed. This is, to the best of our knowledge, the first work assessing plausible in vivo shapes for the absorption spectra of all pigments present within a photosynthetic cell. Results are validated with prior literature and highlight the hidden potential of cell absorption spectra when these are properly measured and assessed.

2 Materials and Methods

2.1 Strains and growth conditions

Cells were grown in a 5 liters flat-bed photobioreactor with a surface-to-volume-ratio of 50 m^{-1} and a depth of 4 cm at constant pH of 7.0 and temperature value of 30 $^{\circ}$C in continuous operation after they were inoculated (J.-H. Kwon, Rögner, and Rexroth 2012). Cell density was kept constant under turbidostatic process control. Cells were cultivated for at least 48 hours till a constant growth rate was established.

We analyzed *Synechocystis* cultures, namely the wild-type (WT) strain and two truncated phycobilisome (PBS) mutants, Olive (Rögner, Nixon, and Diner 1990) and PAL (Ajlani and Vernotte 1998), to obtain their specific absorption spectra in stable photobioreactor conditions to ensure that organisms were acclimated to the same intensity in sufficient time. To this purpose, absorbance spectra within the PAR range were measured at every nanometer after cultivating cells at 100 µmol photon $\cdot m^{-2} \cdot s^{-1}$ of cool white LED lamp. After stabilization of the culture at an OD_{750} value of 0.5, a sample was taken to measure absorbance of the cells.

Optical measurements of the samples were performed by means of a Shimadzu UV2450 UV-vis spectrophotometer equipped with an integrating sphere for absorbance measurements and 1-cm depth cuvettes. The latter device is a double-beam system with an integrating sphere ISR-2200 whose internal diameter is 60 mm with $BaSO_4$ -inside coating.

The cell number of each culture was determined using the Z2 Coulter particle count and size analyzer from Beckman Coulter. 20 µl of a cell culture were diluted in 10 ml Isoton II buffer solution and added to the counter. The

chlorophyll content was calculated according to (Porra, Thompson, and Kriedemann 1989). Three biological replicates were used for obtaining the mean value of each magnitude.

2.2 In vitro absorption spectra of photosynthetic pigments

The principal light-harvesting structures (and their photosynthetic chromophores) in *Synechocystis* are the phycobilisome rods (phycocyanin), the phycobilisome core and terminal-emitter (allophycocyanin) (Kondo et al. 2007), several carotenoids and the photosystems (principally chlorophyll a). The main carotenoids in this organism are β-carotene, zeaxanthin, echinenone, myxoxanthophyll and 3' – hydroxyechinenone (Takaichi, Maoka, and Masamoto 2001). Other special chromophores like red-shifted chlorophyll molecules, the reaction centers of each PS together with their so called primary electron acceptors and pheophytin molecules can also be found (Gobets et al. 2003). Pigment cell location, main chromophores and assessed strains are shown in Fig. 1A.

Photosynthetic pigments are known to have red-shifted absorption spectra under physiological conditions. For example, the shift of carotenoids is between 10 and 25 nm depending on the employed solvent (Kakitani, Honig, and Crofts 1982). Interestingly, for some mutant strains and extreme environmental conditions, carotenoid expression can be largely promoted and related absorption peaks can be distinguished when cellular absorption is measured. This is the case for *Synechocystis* strains under nitrogen starvation (von Wobeser et al. 2011), as under such conditions minor peaks appear at 485 and 520 nm, The first peak corresponds to the presence of β-carotene and zeaxanthin, the second to myxoxanthophyll.

Such phenomenon simplifies the wavelength shift of in vitro spectra to converge with the in vivo related spectra. For chlorophyll a, its spectrum was linearly displaced between both peaks: the blue maximum was positively shifted 8 nm, whereas the red one was displaced 18 nm. This linear and progressive shift is plausible if one compares the oscillatory trend of chlorophyll a in vitro and the one corresponding to the absorption spectra of species with only chlorophyll a as main light-harvesting pigment within the yellow-to-red wavebands. To estimate each chromophore concentration, specific absorption spectra of individual pigments within solvents are needed: such data imply not just the relative spectral distribution but also its absolute magnitude. Usually, the only value reported in literature is the extinction or specific absorption coefficient at the characteristic peak wavelength of the absorption signature. In our case, we chose data gathered with a reference solvent such as acetone due to an extensive amount of available pigment

data (Wright, Jeffrey, and Mantoura. 1997). Henceforth, all chromophore information is referenced to this solvent with the exception of the echinenone extinction coefficient (petroleum ether) and the phycobiliproteins, whose absorption was measured from purified phycobilins and, in particular, from purified trimer complexes in the case of allophycocyanin (MacColl 2004). All starting in vitro absorption signatures and their properties, including the inferred wavelength shift, are detailed and referenced in Table 1.

Despite most of the in vitro spectra are well characterized in previous works, there are few extinction coefficients that had to be imposed due to literature unavailability. In the case of the 3'-hydroxyechinenone molecule, which is the main chromophore of the orange carotenoid, the absorption signature of that protein was assumed to this purpose (Chábera et al. 2011) and the value of the echinenone extinction coefficient assumed. With respect to the phycobilins conforming the phycobilisomes, it has to be noted that there is an inversely proportional relationship between that protein content and the absorption coefficient. Prior works suggest that the values at the peak wavelength in vivo for PC lie in the range 0.004 to 0.008 $m^2 \cdot mg^{-1}$ (Simis and Kauko 2012), though for some phytoplankton species this number is reported to be just below 0.003 (Yacobi et al. 2015). The concentration of phycocyanin in our strain is higher than the content in any of such species, hence an even lower coefficient is expected. To reconcile such magnitude uncertainty, we decided to assign a value of 0.0027 $m^2 \cdot mg^{-1}$ to the phycocyanin weight-specific absorption coefficient and 0.0029 to its allophycocyanin partner. The latter number arises from the molar extinction coefficient ratio of the protomer (αβ) in each phycobiliprotein at their highest absorption peak (Rakhimberdieva et al. 2001) and taking into account that the protomer weight in phycocyanin and allophycocyanin is 35.0 and 29.6 kDa, respectively (Bryant, Glazer, and Eiserling 1976).

Red chlorophyll contribution was also included since there are 3 molecules per PSI complex *Synechocystis* and 4 to 5 if it is a trimeric structure (Gobets and Van Grondelle 2001), but its absorption is partly located in the infra-red band, i.e. outside the PAR, with a peak at room temperature located at 702 nm. For simplicity, we supposed an identical shape than bulk chlorophyll a molecules but with the whole spectrum shifted to match the given peak wavelength. Reaction centers (RCs) of PSI and of PSII, which are formed by special chlorophyll a dimers, were also taken into consideration and their absorption maxima situated at 698 and 680 nm, respectively. The primary acceptor of PSI, absorbing at a maximum of 686 nm, and pheophytin of PSII were also included.

Since some of the special molecules are located in a specific type of photosystem, the PSI:PSII ratio has to be taken into account for each strain. It is worthwhile noting that most of the cell chlorophyll content is associated with

PSI since PSI:PSII ratios lie in the range 4-6 in the WT strain (Moal and Lagoutte 2012; Tian et al. 2011). Therefore, assuming a PSI:PSII ratio of 5 in the WT under moderate light conditions and a number of chlorophyll molecules of 96 (Jordan et al. 2001) and 35 (Umena et al. 2011), respectively, around 90% of the chlorophyll a content is located in PSI complexes in WT. The PS ratio in Olive and PAL was hypothesized to be 1.5 and 1, respectively (J. H. Kwon et al. 2013). For the reconstruction of the PSI absorption spectrum, it was assumed that in each PSI complex, there are 22 β-carotene molecules, eight of echinenone and one of zeaxanthin (Vajravel et al. 2016).

2.3 Reconstruction of the absorption spectrum

The procedure for reconstructing the in vivo absorption spectrum of *Synechocystis* cells from the specific coefficients of the respective spectra in organic solvents (aqueous buffer solution for phycobilins) will be outlined. The aim of this procedure is to assess the real absorption spectrum of all present pigments through the reconstruction of the true cell signature. In vitro spectra of all light-harvesting chromophores were first defined, that is, quantified in absolute-mass units and red-shifted to match cell absorption peaks. In this context, pigment absorption coefficients under physiological conditions cannot be considered as unequivocal magnitudes because light capture in the chromophores depends on the cell geometry, size and the amount of harvesting compounds (Bricaud and Stramski 1990; Greg Mitchell and Kiefer 1988), phenomenon known as package effect (Morel and Bricaud 1981). Therefore, they have to be corrected with the former magnitude (Detailed information on the calculation of the package-effect derivation can be found in the Supplemental Material). The mathematical equation describing the spectrum reconstruction can be expressed as:

$$a^*(\lambda, p, i) = a_{sol}(\lambda, p) \cdot Q_a^*(\lambda, i) \cdot c(p, i) \cdot s(\lambda, p) \quad (1)$$

$$a^*(\lambda, i) = \sum_{p=1}^{p=N} a^*(\lambda, p, i) \quad (2)$$

Being $a^*(\lambda, p, i)$ the absorption coefficient (m^{-1}) of the pigment *p*, in the strain *i* at the wavelength λ. Despite the departing in vitro weight-specific pigment signature $a_{sol}(\lambda, p)$ is identical for all strains, the corresponding strain package effect $Q_a^*(\lambda, i)$ and the pigment concentration $c(p, i)$ are not. The fitting coefficient $s(\lambda, p)$ represents the pigment-signature modifications that are needed to satisfactorily reconstruct the cell spectrum. This correction factor is strain-independent and it emerges, among other opto-physical phenomena, from the heterogeneity of protein

structures surrounding the chromophores unlike in vitro conditions in which pigments are homogeneously dispersed in solvents. The matching procedure was achieved by manually fitting the resulting sum of the *N* pigment spectra to the true absorption spectrum of each of the three strains, $a^*(\lambda, i)$. In an iterative manner, we can obtain the pigment concentration $c(p, i)$ and necessary spectrum modifications $s(\lambda, p)$ to match each strain spectrum. Finally, the in vivo weight-specific pigment spectra $a^*_{vivo}(\lambda, p)$ result from applying the fitting factor $s(\lambda, p)$ to the in vitro spectra $a_{sol}(\lambda, p)$:

$$a^*_{vivo}(\lambda, p) = a_{sol}(\lambda, p) \cdot s(\lambda, p) \quad (3)$$

Remarkably, the absorption coefficients in physiological conditions $a^*_{vivo}(\lambda, p)$ are assumed to be strain-independent and their overall magnitude, given by the mean weight-specific coefficient, equal to the corresponding in vitro value.

2.4 Light absorption assessment and further excitation transfer

The quanta absorbed by each cell (or pigment) can be estimated through its absorption spectrum as it indirectly represents the probability of absorbing radiation at any given wavelength. Assuming a stable optical phenotype that concurs with the supposed absorption spectrum, any light source can be studied because absorption is an inherent optical property. The specific (in our case chlorophyll-specific) absorbed photon flux of a cell (or a pigment) can be computed by multiplying the absorption spectrum by the emission one of the light source:

$$\sigma(\lambda)_{C,PFD} = a^*_c(\lambda) \cdot PFD(\lambda) \quad (4)$$

where $\sigma(\lambda)_{C,PFD}$ denotes the specific-absorbed photon flux distribution (PFD) of the entity C under a light source defined by its PFD within the PAR range and $a^*_c(\lambda)$ is the specific-absorption coefficient. Thus, $\sigma(\lambda)_{C,PFD}$ corresponds to the amount of harvested light per unit of chlorophyll and time at each wavelength (µmol photon · mg chl $a^{-1} \cdot s^{-1} \cdot nm^{-1}$). Further, the area below the *PFD(λ)* (µmol photon · $m^{-2} \cdot s^{-1} \cdot nm^{-1}$) represents the total irradiance

(µmol photon · m^{-2} · s^{-1}). The specific-absorbed photon flux distribution can be integrated up to an overall value, the mean specific-absorbed irradiance (µmol photon · mg chl a^{-1} · s^{-1}) via the Equation (5):

$$\bar{\sigma}_{C,PFD} = \int_{\lambda_0=400}^{\lambda_1=700} \sigma(\lambda)_{C,PFD} \cdot d\lambda \quad (5)$$

Similarly, one can compute the mean specific-absorption cross-section (m^2 · mg chl a^{-1}) of the cell (or any chromophore) leveraging the source PFD as a weight factor (area of one unit) and using Equations (4) and (5).

Alternatively, to further calculate the amount of photons arriving at each photosystem and, by doing so, to estimate the growth potential, the amount of carotenoid and chlorophyll molecules attached to each photosystem has to be considered. The number of chlorophyll a molecules assumed in each PSI and PSII monomer and the PS ratio of each strain are the ones previously considered. PBS antennas are assumed to transfer their excitation with an efficiency close to 100% to each PS. β-carotene is rather abundant in cyanobacteria and the only carotenoid whose energy transfer capacity to the reaction centers has been already proofed (Cerullo et al. 2002). It was hypothesized that 75% of all β-carotene molecules are found in the thylakoid membrane (Vajravel et al. 2016). Moreover, their amount is 22 molecules in each PSI (Jordan et al. 2001) and 11 in PSII (Umena et al. 2011).

3 Results

3.1 Reconstruction of the cell absorption spectrum

To address any question regarding pigment concentration and spectrum reconstruction, the first calculation that can be directly carried out is the package effect. The measured mean external diameter of the WT, Olive and PAL cell d_e were 1.95±0.04, 1.87±0.06 and 1.85±0.03 µm, respectively, while the chlorophyll mass per cell averagely accounts for 30.2±2.5, 27.0±3.1 and 15.8±1.4 fg in each strain. Periplasmic space to calculate the internal diameter d_i and the cell size distribution are also needed (as indicated in the Supplemental Material). As expected, the package effect is inversely proportional to the absorption coefficients (Supplemental Fig. S1). So, in the spectral regions where the absorption is lesser, such as for green radiation, the package effect is negligible in all strains, whereas for blue color the high pigment density can lead up to a 22% and 26% reduction in the effective absorption of the WT and Olive

light-harvesting compounds, respectively.

The reconstruction of the true in vivo absorption can also be achieved by means of deconvolution techniques using Gaussian curves that emulate chromophores. However, this method does not allow a proper spectral identification of the pigment absorption due to their distinctive non-normal spectra (Supplemental Fig. S2). Alternatively, following the proposed pigment-signature approach (Fig. 1B), cell and in vivo pigment spectra were computed. Reconstructed in vivo chlorophyll-specific absorption spectra at 30 ◦C for WT (Fig. 2), Olive (Fig. 3A) and PAL (Fig. 3B) strains are shown. Bulk chlorophylls and photosystem-associated molecules are displayed with blue color in all figures showing spectral properties throughout this work. In particular, reaction centers, associated molecules and red-shifted chlorophylls in PSI are also considered, but their overall contribution is practically negligible in this organism in the photosynthetically active radiation (PAR) range. Similarly, green color is used for all carotenoids, while red is employed for phycocyanin and yellow for allophycocyanin

Remarkably, the calculated in vivo spectrum for all strains matches the experimental one for the whole PAR range. Around 470 nm, β-carotene, zeaxanthin, echinenone, PSI reaction centers and red-shifted chlorophyll a molecules contribute to a less negative absorption slope in WT. At 490-500 nm, a shoulder appears which is due to β-carotene and zeaxanthin, together with one peak of myxoxanthophyll. The phycocyanin signature displays a shoulder-turning point in the yellow region, around 575 nm. There is an absorption valley for the red radiation which is derived from the absorption behavior of the phycobilin and the chlorophyll a, owning the allophycocyanin chromophores its peak at 660 nm. The absorption at 700 nm is slightly enhanced due to the presence of a pool of red-shifted chlorophyll a molecules (702 nm) and the reaction centers (698 nm), both in the PSI complexes. The absorption contribution of different photosystem (PS) chromophores is shown in detail for the shortest-wavelength region of the spectrum (inset plot of Fig. 2)

The evaluation of the Olive absorption spectrum proceeds in a similar way (Fig. 3A). The blue-peak shape is slightly modified due to the higher carotenoid content per chlorophyll, which can be appreciated in the carotenoid band: the band is higher and local turning points appear that correspond with several pigment peaks. The green-absorption decay is sharper due to the higher content of those molecules and almost linear in our case. This strain shows some minor absorption bumps for yellow-to-orange light that are consistent with the allophycocyanin and chlorophyll a absorption. The red peak is slightly higher and broader than in WT due to a greater allophycocyanin content per chlorophyll.

Finally, PAL strain (Fig. 3B) shows a similar trend regarding the carotenoids. Their content is higher and so, the blue-peak shape changes and its maximum is higher. The absorption decay is more pronounced and the minimum is similar to Olive. The cell signature for the longest wavelengths basically follows the absorption-spectrum of chlorophyll a, but it needs some minor contribution of phycobilins and the other chlorophyll related molecules to fully match it. Regarding the package effect, its impact can be appreciated when considering two strains, e.g. the shape of the chlorophyll a spectrum at 439 nm is very similar but not identical in Olive than in PAL.

The comparison between original in vitro and the estimated in vivo spectra is also outlined (Fig. 4). The former have been displaced so that they coincide with the assumed peak wavelengths in physiological conditions. Both types of spectra for all pigments can be found as text file in the Supplementary Material. In particular, in vitro chlorophyll a signature has been linearly shifted as described in the Materials and Methods section. Regarding the carotenoids, only β-carotene and myxoxanthophyll are depicted as zeaxanthin has a close absorption spectrum to the carotene one. In addition, echinenone's signature has a rather round contour and no significant smoothing was applied (not shown). Spectra are rounder and slightly more distributed, especially for the case of carotenoids. Phycocyanin has a broader absorption in the red region and higher values in the purple one in comparison with the original signature. On the contrary, allophycocyanin presents a lower harvesting capacity in the green-to-orange range. The spectrum of chlorophyll is more distributed, but its shape remains almost identical to that measured in acetone solvent. Different chlorophyll a in vivo absorption spectra postulated by several research groups are also schemed (inset plot of Fig. 4): Wozniak (Woźniak et al. 2003), Hoepffner (Hoepffner and Sathyendranath 1991), Zhang (Zhang et al. 2017), Bricaud (Bricaud et al. 2004) and Bidigare (Bidigare et al. 1990). Our proposed signature for chlorophyll a is close to Bidigare's proposal.

3.2 Quantification of the pigment concentration

For validation of the pigment estimation (Fig. 5), only wild-type data are available and hence this strain serves as a reference for the in silico predictions. Regarding the phycobiliproteins, we found two contributions where such proteins were quantitatively determined in *Synechocystis* WT. For PC, works report values between 6.5 and 7.5 mg · mg chl a^{-1} (Touloupakis, Cicchi, and Torzillo 2015; Tsunoyama et al. 2009). APC concentrations are reported to be below 2.0 mg · mg chl a^{-1}, while our estimation accounts for almost 2.0 mg · mg chl $a^{-1.}$ The prediction of the

carotenoid content in WT also lies within the range of minimal and maximal values reported in previous research using HPLC analysis (Kłodawska et al. 2015; Lagarde and Vermaas 1999; Lindblad et al. 2019; Takaichi, Maoka, and Masamoto 2001; Vajravel et al. 2016; Zakar et al. 2017). The calculated amounts are in agreement with reported values: β-carotene 0.111, zeaxanthin 0.075, echinenone 0.050 and myxoxanthophyll 0.085 mg · mg chl a^{-1}. The relative mass proportions of the carotenoids are 34%, 22%, 15%, 25% and 4% for 3'- hydroxyechinenone. All carotenoids add up to a global amount of 0.334 mg · mg chl a^{-1}.

For the Olive strain, we estimate the allophycocyanin amount to be in the range of 3.4 mg · mg chl a^{-1}. A similar relative increase is found for total carotenoid mass (62%) to account up to 0.53 mg · mg chl a^{-1}. The carotenoid composition is practically identical in relative units to the WT proportions, but β-carotene and zeaxanthin are approximately 10% more abundant and myxoxanthophyll 10% less. PAL strain presents traces of phycobilin proteins, around 3% of the WT value for PC and virtually zero for APC. Total carotenoid is predicted to be 0.65 mg · mg chl a^{-1}, with a relative increase of β-carotene and zeaxanthin of roughly 30% and 50% with respect to the WT proportions.

3.3 Reconstruction of other absorption spectra

Once pigments signatures are unraveled, it is possible to reconstruct the absorption spectra of light-harvesting structures such as the photosystems or the phycobilisomes. The experimental and the computed spectrum of both structures in *Synechocystis* are plotted (Fig. 6). All spectra are normalized to the maximum peak. PSI signature has been assumed to be formed by the absorption contribution of bulk chlorophyll a molecules, the reaction centers, the pool C702 of red-shifted chlorophylls and three carotenoids in the mass proportions given by a prior work as detailed in the Material and Methods Section. The simulated spectrum (Fig. 6A) is located between the experimental one for the monomeric and for the trimeric state (Gobets et al. 2003) within most wavelengths with the exception of the carotenoid band. The red-to-infrared spectral region and the contribution of each molecule to PSI absorption are also plotted (inset plot of Fig. 6A). Analogously, the reconstructed and experimental spectrum (Zlenko et al. 2019) of the phycobilisome are depicted (Fig. 6B). Again, the in silico prediction is almost identical to the recently published PBS spectrum for this strain.

Alternatively, computed pigment signatures can be used in a versatile manner for studying other published absorption spectra. The experimental chlorophyll-specific absorption spectra for *Synechocystis* WT cultures

acclimated to three different irradiance levels (Kopečná et al. 2012) were reconstructed. The computed cell spectrum was calculated by gathering pigment concentration via least-squares optimization and resembles much the original spectra (Supplemental Fig. S3). A fourth experiment was also carried out in that work where *Synechocystis* absorption spectra were measured at different time periods to check spectrum evolution between a low and a high irradiance level. The corresponding pigment evolution for the bilins and the carotenoids are also represented (inset plot of Supplemental Fig. S3). While chlorophyll a-specific content of allophycocyanin remains constant, that of phycocyanin gets reduced at higher intensities and alternatively, carotenoid amounts are increased several times.

Finally, a cell-extract absorption reconstruction of a *Synechoccocus* strain was also performed. In this case, we do not depart from the estimated in vivo pigment signatures, but acetone ones are applied, i.e. no shift, nor smoothing neither package-effect calculation is required. Relative absorption coefficients with respect to the red peak are shown for three different light intensities (Supplemental Fig. S4). Our predictions are compared with published spectra of *Synechococcus* OS' extracts in acetone (Kilian et al. 2007). This strain is supposed to own β-carotene, zeaxanthin and a myxoxanthophyll-like compound. Again, the in silico absorption spectra are also very similar to the experimental ones despite the uncertainty of the myxoxanthophyll-like signature.

3.4 Absorption cross-section under different illumination environments

Knowing the cell (or any pigment) absorption signature, the rate of light-harvesting, i.e. the specific-absorbed photon flux, experienced by the cell (or any chromophore) can be estimated. It represents the absorption capacity of photons per mass unit and time at any wavelength. The corresponding WT's magnitude has been plotted (solid black, Fig. 7) for our LED lamp. Its shape is a result of multiplying both spectra: lamp emission (dashed black) and cell absorption (dotted black). The absorption rate is logically higher for blue radiation, waveband at which both spectra display greater values and thus a sharp peak is visible. For the rest of wavelengths, the absorbed radiation is much lower because at these wavelengths either the absorption or the emission level is small.

Similarly, other light sources can be evaluated regarding the specific-absorbed photon flux. For short periods of exposure time, cells do not have time to acclimatize to the new optical condition and original absorption properties

remain. Supplemental Fig. S5 comprises twelve illumination environments, whose emission spectra are displayed with colored areas following the corresponding wavelengths. The first six sources own broad signatures: solar light and five white spectra (incandescent light bulb, fluorescent lamp, halogen lamp, cool and warm white LEDs). The latter six are Gaussian LED lamps with different mean wavelengths (blue 440, turquoise 480, green 550, amber 590, orange 624 and red 674, all in nm) but same deviations, thus equally shaped. So, the specific absorption rate was as well computed for each of the twelve sources as calculated for the cool white LED lamp. Again, only where emission and absorption spectra are high, the harvesting rate is large as well (Supplemental Fig. S6). Under Gaussian light, the specific-absorption rate owns the same shape as the emission one due to its shape narrowness.

In general, the area below the absorbed photon flux represents the total amount of harvested quanta per unit of chlorophyll (or equivalently per cell) and time ignoring the wavelength distribution, i.e. the total absorbed irradiance. Hence, if we assume the lamp emission to be a weight distribution, owning an area of one unit, the mean absorption cross-section for each light-harvesting compound can be computed. In this regard, the mean cellular specific-absorption cross-section of *Synechocystis* WT is split into each pigment cross-section for the analyzed light sources and short-term experiments (Fig. 8). For the solar illumination and the white lamps, the mean absorption cross-section for the whole PAR range is around 0.013-0.017 $m^2 \cdot mg\ chl\ a^{-1}$, while for monochromatic LED lamps dissimilar results are obtained. In this respect, green and amber lamps lead to lower light-harvesting capacities per chlorophyll a unit than for white lamps. Moreover, under turquoise and red LED light harvesting is slightly higher but carotenoids contribute the most in the first case. In particular, under blue and orange light *Synechocystis* absorption is the highest, 0.029 and 0.020 $m^2 \cdot mg\ chl\ a^{-1}$, respectively, since the main cellular peaks overlap the LED emission ones. Remarkably, for blue and red light most of the radiation is absorbed by chlorophyll a present in PSI units, roughly 50-70% for each case, whereas under orange radiation PBS are responsible for the majority of the light capture, reaching values up to 85% of the overall radiation. Noteworthy, the lamp emission will change along the optical path-length when cell density is not very low and thus, it will be a function of the depth, i.e. with varying intensity and spectrum. For simplicity, we have only assessed the cross-sections and absorbed flux distribution for the original light-source spectrum. Knowing the remaining available radiation, one can analogously proceed and similarly estimate the assessed magnitudes of this section.

3.5 Color light-limited growth assessment

Mean absorption cross-sections at any wavelength along the PAR range can be similarly estimated. To do so, we utilized as emission spectrum a Gaussian-shaped LED lamp centered at each entire-value wavelength with a dispersion waveband of 10 nm. After computing each cross-section, the spectrally dependent growth of any *Synechocystis* strain can be roughly assessed. Thus, several suppositions have to be considered: first of all, the radiation is assumed to be the main limiting factor. Second, the quantum yield does not depend on the light color. Third, we neglect the color effect on pigment composition for simplicity. Finally, other phenomena that could alter growth values, such as NPQ or photodamage, are omitted because in our proposed set-up light is a limiting factor.

The estimated growth capacity for each strain is depicted (Fig. 9A). One reference providing with photosynthesis-quantum-yield data for the WT strain is also shown (Tyystjärvi et al. 2002). For comparison, growth rates have been normalized to the maximal value of WT, which occurs at 625 nm. The PSII/PSI proportion for each optical mutant, indicated in the Methods section has been assumed, as well as the measured chlorophyll content. Remarkably, the potential for biomass creation is hypothesized to be the sum of quanta absorbed by chlorophyll a in PSII plus those harvested by all PBS-antenna chromophores when the joint amount of both structures is lower than the total irradiance captured by all chlorophyll-type pigments placed in PSI units ($\sigma_{PBS} + \sigma_{PSII} < \sigma_{PSI}$): the cell is locked in state 1, e.g. under blue light. Alternatively, when initial phycobilisome and PSII absorption is higher than the PSI light-harvesting capacity ($\sigma_{PBS} + \sigma_{PSII} > \sigma_{PSI}$), the cell reconfigures the thylakoid membrane so that part of the PBS antennas can direct energy to PSI complexes to maximize the growth (Joshua and Mullineaux 2004), i.e. the organism tries to equalize the excitation input: the cell shifts to state 2, e.g. under orange light.

Regarding the computed growth potential, for cyan-related colors the cell is not efficient (growth values slightly above 10% of the maximum rate) since most of the light is captured by carotenoids, which are not proven to transmit energy efficiently to reaction centers with the exception of β-carotene. For greater wavelengths, the biomass formation is higher due to the appearance of PBS absorption up to a maximal value around 625 nm. For higher wavelengths, overall PBS absorption decreases and so the growth potential. The displayed experimental data support our biomass prediction for most colors, but growth under red light is underestimated.

With respect to Olive productivity, it can create a similar biomass quantity to the WT case under blue light because the excitation is better distributed between both photosystems due to a more equilibrated PS ratio. However, the lack

of phycocyanin is a great disadvantage under low irradiance for yellow and orange colors. The increased amount of allophycocyanin is not enough to compensate such loss. Therefore, this strain cells approximately grow less than half than the WT ones under yellow and orange radiation. These figures are in agreement with the data reported in (J. H. Kwon et al. 2013) where Olive mutant grows less than WT under low-light conditions. Finally, PAL shows a reduced biomass formation for any color due to the lack of PBS antennas. It displays similar growth rates to WT under blue light, as measured in a recent research (Luimstra et al. 2019) because its higher PSII/PSI ratio can compensate the phycobilisome loss under this radiation.

The upper curve (yellow graph in Fig. 9B) illustrates in WT the initial energy imbalance B among photosystems for any PAR wavelength assuming all PBSs are initially attached to PSII complexes. The final state after state-transition is also displayed (state 2 above balance line, state 1 below). So, negative values of B imply PSI over-excitation, while positive ones mean that PSII gets initially over-excited due to a higher light harvesting of the bilins. Hence, it is a graphical representation of light color as driving force for state-transitions. The energy balancing can be ascribed to the contribution of the phycobilin absorption to the under-excited PS to equal the excitation arrival in both photosystems. PBS antennas are assumed to transfer their energy at an efficiency close to 100% to each PS and so, they can fully balance the chlorophyll-excitation asymmetry when they absorb enough energy as for the case of green-to-orange radiation. This is state 2, in which PBS share a part of their absorbed energy to PSI, while for state 1, PBS do not harvest enough light and thus, PSI is always over-excited and the PBS-PSI transfer is assumed to be close to zero. Indeed, the estimated amount of PBS-to-PSI transferred energy for optimal biomass creation is computed to be between 35%-45% for most of the state-2 range, i.e. 525-665 nm, but in any case below 50% of the total absorbed energy by the PBS antennas (horizontal-red dashed line in Fig. 9B). Analogously, Olive shows a similar state-2 range that starts around 540 nm and ends up at the same wavelength as the WT (data not shown). Nonetheless, the amount of phycobilin excitation derived to PSI needed for PS equilibrium is lower, below 25% because of the smaller PBS absorption arisen from the PC loss. PAL displays no state-transitions because it lacks of functional PBS structures.

4 Discussion

In this research, we reconstructed the absorption spectrum of several optical mutants of a cyanobacterial cell from

solvent-pigment signatures. Despite in vivo pigment spectra were retrieved via a fitting procedure, they do not display any strange contour and are rather congruent with respect to original signatures (Fig. 4). Moreover, the in vivo weight-specific pigment absorption coefficients a^*_{vivo} are strain-independent. Alternatively, it could be in principle possible that some unknown pigments are not included in this assessment and therefore the true pigment spectrum might be different and the real concentration of assumed pigments lesser. Indeed, a novel type of PBS lacking APC has been recently discovered (Liu et al. 2019), but its structure and abundance remains unclear. So, there is no evidence in prior literature supporting the presence of other main chromophores in this organism. Moreover, there is an overlap of various pigments for some wavebands, especially for the carotenoids and the phycobilins with respect to the chlorophyll. Hence, we cannot discard that the true signature may be slightly different, but we expect it to be close to the proposed ones. Otherwise, pigment spectra would display artificial shapes or cell-spectrum reconstruction would be not possible. Interestingly, smoothed pigment spectra are needed to adequately obtain the true in vivo spectrum, being these modifications rather small in magnitude terms and also regarding spectral distribution for most of the chromophores. In other words, computed signatures in physiological conditions bear a close resemblance to the spectra in solvents.

The pigment-content estimation is another relevant outcome from the reconstruction procedure. For the WT strain, we are able to predict within a reasonable precision the concentration of the main light-harvesting compounds present in the cell (Fig. 5), while gathering an absorption spectrum that is very close to the true cell one (Fig. 4). We obtained a carotenoid and bilin concentration within literature range.

For Olive-antenna mutant, no phycocyanin is expected. To compensate for such loss, this strain enhances the production of cores. The allophycocyanin content enlargement concurs well with previous figures on protein content within the thylakoid and soluble fraction of Olive with respect to the WT (J. H. Kwon et al. 2013). An increase of 60% of core units seems plausible in terms of spatial requirements because the volume of the APC cores is lower than that of entire phycobilisome structures. In the original PAL-design article (Ajlani and Vernotte 1998), it was claimed that a very small amount of phycobilins might be present in the cytoplasm, yet not active. Moreover, traces of both subunits of phycocyanin were found in a previous work in this strain (J. H. Kwon et al. 2013). Thus, further work is needed to unravel whether these traces of bilins are functional in PAL as our model suggests.

The cool white LED lamp offers a good balance between chlorophyll a and bilin absorption, yet part of the energy is wasted as it is green radiation that can hardly be absorbed. Further, a big proportion of photons are captured by

carotenoids and thus transformed into heat and fluorescence but not into an effective electron flow. Alternatively, simply by choosing a warm white LED, we would expect higher growth rates since most of the light can be absorbed by the PBSs and no significant absorption by carotenoid is appreciable.

The estimation of the potential growth in WT under low-limiting conditions is in qualitative accordance with published data on photosynthesis quantum yield for different monochromatic light sources. This implies that the assumptions considered under the low-light scenario are fulfilled and that the individual contribution of each pigment to overall absorption is properly assessed. Regarding the excitation distribution, while PBS antenna can redistribute their energy towards both photosystems, there is no clear mechanism through which PSI can divert its excess energy towards PSII. Reverse spillover has been proposed as a hypothetical strategy that could explain this phenomenon (Zhao et al. 2015), but there is no solid evidence supporting this mechanism. On the contrary, state transitions have been deeply studied and are supposed to reallocate the excess energy among photosystems shifting the cell between state 1 and 2, when necessary. This is the reason why *Synechocystis* and organisms owning similar phycobilisome antennas can grow faster under yellow-orange light than under blue radiation, as our theoretical growth curve indicates (blue curve in Fig. 9B).

5 Conclusion

In this research, we showed that it is feasible to reconstruct the in vivo absorption spectrum of diverse optical mutants of a cyanobacterial cell by using the signatures of the individual pigments present in these strains. In general, the pigment absorption spectra tend to be broader and display less pronounced local maxima in physiological conditions. These smoothing effects have been already visualized in spectra of pigments placed in high-polarizability solvents and those obtained with photo-acoustics procedures. This phenomenon results from a slightly different absorption spectrum of same-type pigments due to their particular molecular interactions with surrounding protein complexes. So, the overall pigment spectrum is the sum of the all chromophore spectra for each pigment case. Additionally, pigments absorb light in a similar manner to the in vitro conditions in terms of magnitude and spectrum. The assumption that the mean weight-specific absorption coefficient is very similar in physiological and in vitro

conditions seems to be plausible. Indeed, the predicted pigment content is in agreement with published values in the wild-type. Moreover, the absorption spectrum of several photosynthetic structures and further strains were also adequately reconstructed. We also evaluated the color impact on cellular growth when light is the main limiting factor. Orange-red radiation supports maximal growth under such conditions due to efficient photosystem-energy-balance via state-transitions and relatively high absorption coefficients.

Future research will cope with the assessment of absorption spectra under other growth conditions like high-irradiance stress or nutrient deprivation in order to quantify the chromophore content, check the cell physiology at diverse experimental conditions and evaluate other processes such as chromatic adaptation. Further, it could be useful to investigate the absorption of other species under the described modeling framework to verify if the pigment shape and light-harvesting capacity are maintained among organisms. Moreover, the proposed methodology can be coupled to a mechanistic photosynthesis model that incorporates photons as the input for the excitation-energy transfer and consequent electron flow. The distribution of the excitation formation inside the cell can shed light on the fate of such energy and so, on how spectral properties can affect the physiology of the photosynthetic organism.

This contribution exemplifies the capacities of mathematical modeling under given hypotheses and physical laws. It describes a novel strategy to unlock the potential of cell absorption spectra since they can be gathered in a non-invasive manner and contain relevant information on the cell state. Analogous reconstruction frameworks have been already proposed for oceanographic applications. But, to the best of our knowledge, there is no piece of research satisfactorily reconstructing the absorption spectrum of a photosynthetic organism from individual pigment spectra. By doing so, this research turns out to be the first one delivering plausible in vivo shapes for the main light-harvesting compounds present inside a photosynthetic cell. Thus, it offers a systematic way of obtaining pigment concentrations and a more comprehensive view on the fate of absorbed energy and its implications for photosynthesis processes.

6 Acknowledgements

We kindly acknowledge Alberto Conejero for his suggestions on the modeling part.

Compliance with ethical standards

Conflict of interest. The authors declare no conflict of interest.

References

Aasen, A. J., and S. Liaaen Jensen. 1966. “Carotenoids of Flexibacteria. IV. The Carotenoids of Two Further Pigment Types.” *Acta Chemica Scandinavica* 20(8): 2322–24. http://actachemscand.org/doi/10.3891/acta.chem.scand.20-2322 (March 31, 2020).

Ajlani, Ghada, and Claudie Vernotte. 1998. “Construction and Characterization of a Phycobiliprotein-Less Mutant of Synechocystis Sp. PCC 6803.” *Plant Molecular Biology* 37(3): 577–80. https://link.springer.com/article/10.1023/A:1005924730298 (March 31, 2020).

van Amerongen, Herbert, Rienk van Grondelle, and Leonas Valkunas. 2000. Photosynthetic Excitons *Photosynthetic Excitons*. World Scientific. https://www.worldscientific.com/worldscibooks/10.1142/3609 (March 28, 2020).

Bennett, Allen, and Lawrence Bogobad. 1973. “Complementary Chromatic Adaptation in a Filamentous Blue-Green Alga.” *Journal of Cell Biology* 58(2): 419–35. https://rupress.org/jcb/article/58/2/419/18179/COMPLEMENTARY-CHROMATIC-ADAPTATION-IN-A (March 31, 2020).

Bidigare, Robert R., Michael E. Ondrusek, John H. Morrow, and Dale A. Kiefer. 1990. “In-Vivo Absorption Properties of Algal Pigments.” In *Ocean Optics X*, SPIE, 290. https://spie.org/Publications/Proceedings/Paper/10.1117/12.21451 (March 31, 2020).

Bricaud, Annick, Hervé Claustre, Joséphine Ras, and Kadija Oubelkheir. 2004. “Natural Variability of Phytoplanktonic Absorption in Oceanic Waters: Influence of the Size Structure of Algal Populations.” *Journal of Geophysical Research* 109: C11010. http://doi.wiley.com/10.1029/2004JC002419 (March 31, 2020).

Bricaud, Annick, and Dariusz Stramski. 1990. “Spectral Absorption Coefficients of Living Phytoplankton and Nonalgal Biogenous Matter: A Comparison between the Peru Upwelling Areaand the Sargasso Sea.” *Limnology and Oceanography* 35(3): 562–82. http://doi.wiley.com/10.4319/lo.1990.35.3.0562 (March 31, 2020).

Bryant, Donald A., Alexander N. Glazer, and Frederick A. Eiserling. 1976. “Characterization and Structural

Properties of the Major Biliproteins of Anabaena Sp." *Archives of Microbiology* 110(1): 61–75. https://link.springer.com/article/10.1007/BF00416970 (March 31, 2020).

Buschmann, C., and E. Nagel. 1993. "In Vivo Spectroscopy and Internal Optics of Leaves as Basis for Remote Sensing of Vegetation." *International Journal of Remote Sensing* 14(4): 711–22. https://www.tandfonline.com/doi/abs/10.1080/01431169308904370 (March 31, 2020).

Cerullo, G. et al. 2002. "Photosynthetic Light Harvesting by Carotenoids: Detection of an Intermediate Excited State." *Science* 298(5602): 2395–98. https://science.sciencemag.org/content/298/5602/2395 (March 31, 2020).

Chábera, Pavel et al. 2011. "Excited-State Properties of the 16kDa Red Carotenoid Protein from Arthrospira Maxima." *Biochimica et Biophysica Acta - Bioenergetics* 1807(1): 30–35. https://www.sciencedirect.com/science/article/pii/S0005272810006985 (March 31, 2020).

Collins, Aaron M. et al. 2012. "Photosynthetic Pigment Localization and Thylakoid Membrane Morphology Are Altered in Synechocystis 6803 Phycobilisome Mutants." *Plant Physiology* 158(4): 1600–1609. http://www.plantphysiol.org/content/158/4/1600 (March 31, 2020).

Eng, Denise, and Gladimir V.G. Baranoski. 2007. "The Application of Photoacoustic Absorption Spectral Data to the Modeling of Leaf Optical Properties in the Visible Range." In *IEEE Transactions on Geoscience and Remote Sensing*, , 4077–86. https://ieeexplore.ieee.org/document/4378552 (March 31, 2020).

Faccio, Greta et al. 2014. "Tyrosinase-Catalyzed Site-Specific Immobilization of Engineered C-Phycocyanin to Surface." *Scientific Reports* 4: 5370. https://www.nature.com/articles/srep05370 (March 31, 2020).

Ficek, Dariusz et al. 2004. "Spectra of Light Absorption by Phytoplankton Pigments in the Baltic; Conclusions to Be Drawn from a Gaussian Analysis of Empirical Data." *Oceanologia* 46(4): 533–55.

Fuente, D. et al. 2017. "Light Distribution and Spectral Composition within Cultures of Micro-Algae: Quantitative Modelling of the Light Field in Photobioreactors." *Algal Research* 23. https://www.sciencedirect.com/science/article/abs/pii/S2211926417300371.

Fujiki, T., and S Taguchi. 2002. "Variability in Chlorophyll a Specific Absorption Coefficient in Marine Phytoplankton as a Function of Cell Size and Irradiance." *Journal of Plankton Research* 24(9): 859–74. https://academic.oup.com/plankt/article/24/9/859/1519825 (March 31, 2020).

Gobets, Bas et al. 2003. “Excitation Wavelength Dependence of the Fluorescence Kinetics in Photosystem I Particles from Synechocystis PCC 6803 and Synechococcus Elongatus.” *Biophysical Journal* 85(6): 3883–98. https://www.sciencedirect.com/science/article/pii/S0006349503748036 (March 31, 2020).

Gobets, Bas, and Rienk Van Grondelle. 2001. “Energy Transfer and Trapping in Photosystem I.” *Biochimica et Biophysica Acta - Bioenergetics* 1507(1–3): 80–99. https://www.sciencedirect.com/science/article/pii/S0005272801002031 (March 31, 2020).

Gong, Nan, Zuowei Li, Chenglin Sun, and Zhiwei Men. 2018. “External Field Effect on Electronic and Vibrational Properties of Carotenoids.” In *Progress in Carotenoid Research*, InTech. https://www.intechopen.com/books/progress-in-carotenoid-research/external-field-effect-on-electronic-and-vibrational-properties-of-carotenoids (March 31, 2020).

Green, Beverley R, and William W Parson. 2003. “Light-Harvesting Antennas in Photosynthesis.” *Advances in photosynthesis and respiration* 13: 513. https://link.springer.com/book/10.1007/978-94-017-2087-8 (March 28, 2020).

Greg Mitchell, B., and Dale A. Kiefer. 1988. “Chlorophyll α Specific Absorption and Fluorescence Excitation Spectra for Light-Limited Phytoplankton.” *Deep Sea Research Part A, Oceanographic Research Papers* 35(5): 639–63. https://www.sciencedirect.com/science/article/abs/pii/0198014988900246 (March 31, 2020).

Herbert, Stephen K., Tao Han, and Thomas C. Vogelmann. 2000. “New Applications of Photoacoustics to the Study of Photosynthesis.” *Photosynthesis Research* 66(1–2): 13–31. https://link.springer.com/article/10.1023%2FA%3A1010788504886 (March 31, 2020).

Hertzberg, S., S. Liaaen-Jensen, and H. W. Siegelman. 1971. “The Carotenoids of Blue-Green Algae.” *Phytochemistry* 10(12): 3121–27. https://www.sciencedirect.com/science/article/abs/pii/S003194220097362X (March 31, 2020).

Hiyama, Tetsuo, Mitsuo Nishimura, and Britton Chance. 1969. “Determination of Carotenes by Thin-Layer Chromatography.” *Analytical Biochemistry* 29(2): 339–42. https://www.sciencedirect.com/science/article/abs/pii/0003269769903182 (March 31, 2020).

Hoepffner, Nicolas, and Shubha Sathyendranath. 1991. “Effect of Pigment Composition on Absorption Properties of Phytoplankton.” *Marine Ecology Progress Series* 73: 11–23. https://www.jstor.org/stable/24825388 (March 31,

2020).

Jordan, Patrick et al. 2001. “Three-Dimensional Structure of Cyanobaoterial Photosystem I at 2.5 Å Resolution.” *Nature* 411(6840): 909–17. https://pubmed.ncbi.nlm.nih.gov/11418848/ (November 11, 2020).

Joshua, Sarah, and Conrad W. Mullineaux. 2004. “Phycobilisome Diffusion Is Required for Light-State Transitions in Cyanobacteria.” *Plant Physiology* 135(4): 2112–19. http://www.plantphysiol.org/content/135/4/2112 (March 31, 2020).

Kakitani, T., B. Honig, and A. R. Crofts. 1982. “Theoretical Studies of the Electrochromic Response of Carotenoids in Photosynthetic Membranes.” *Biophysical Journal* 39(1): 57–63. https://www.sciencedirect.com/science/article/pii/S0006349582844901 (March 31, 2020).

Kilian, Oliver et al. 2007. “Responses of a Thermophilic Synechococcus Isolate from the Microbial Mat of Octopus Spring to Light.” *Applied and Environmental Microbiology* 73(13): 4268–78. https://aem.asm.org/content/73/13/4268/article-info (March 31, 2020).

Kłodawska, Kinga et al. 2015. “Elevated Growth Temperature Can Enhance Photosystem I Trimer Formation and Affects Xanthophyll Biosynthesis in Cyanobacterium Synechocystis Sp. PCC6803 Cells.” *Plant and Cell Physiology* 56(3): 558–71. https://academic.oup.com/pcp/article/56/3/558/2461182 (March 31, 2020).

Knoop, Henning, Yvonne Zilliges, Wolfgang Lockau, and Ralf Steuer. 2010. “The Metabolic Network of Synechocystis Sp. PCC 6803: Systemic Properties of Autotrophic Growth.” *Plant Physiology* 154(1): 410–22. http://www.plantphysiol.org/content/154/1/410 (March 31, 2020).

Kondo, Kumiko, Yuriko Ochiai, Mitsunori Katayama, and Masahiko Ikeuchi. 2007. “The Membrane-Associated CpcG2-Phycobilisome in Synechocystis: A New Photosystem I Antenna.” *Plant Physiology* 144(2): 1200–1210. http://www.plantphysiol.org/content/144/2/1200 (March 31, 2020).

Kopečná, Jana, Josef Komenda, Lenka Bučinská, and Roman Sobotka. 2012. “Long-Term Acclimation of the Cyanobacterium Synechocystis Sp. PCC 6803 to High Light Is Accompanied by an Enhanced Production of Chlorophyll That Is Preferentially Channeled to Trimeric Photosystem I.” *Plant Physiology* 160(4): 2239–50. http://www.plantphysiol.org/content/160/4/2239 (March 31, 2020).

Kwon, Jong-Hee, Matthias Rögner, and Sascha Rexroth. 2012. “Direct Approach for Bioprocess Optimization in a

Continuous Flat-Bed Photobioreactor System." *Journal of Biotechnology* 162(1): 156–62. https://linkinghub.elsevier.com/retrieve/pii/S0168165612003690 (March 31, 2020).

Kwon, Jong Hee et al. 2013. "Reduced Light-Harvesting Antenna: Consequences on Cyanobacterial Metabolism and Photosynthetic Productivity." *Algal Research* 2(3): 188–95. https://www.sciencedirect.com/science/article/abs/pii/S2211926413000556 (March 31, 2020).

Lagarde, Delphine, and Wim Vermaas. 1999. "The Zeaxanthin Biosynthesis Enzyme β-Carotene Hydroxylase Is Involved in Myxoxanthophyll Synthesis in Synechocystis Sp. PCC 6803." *FEBS Letters* 454(3): 247–51. https://www.sciencedirect.com/science/article/pii/S0014579399008170 (March 31, 2020).

Lauceri, Rosaria, Mariano Bresciani, Andrea Lami, and Giuseppe Morabito. 2018. "Chlorophyll a Interference in Phycocyanin and Allophycocyanin Spectrophotometric Quantification." *Journal of Limnology* 77(1): 169–77. https://jlimnol.it/index.php/jlimnol/article/view/jlimnol.2017.1691 (March 31, 2020).

Lichtenthaler, Hartmut K. 1987. "Chlorophylls and Carotenoids: Pigments of Photosynthetic Biomembranes." *Methods in Enzymology* 148(C): 350–82. https://www.sciencedirect.com/science/article/pii/0076687987480361 (March 31, 2020).

Lindblad, P. et al. 2019. "CyanoFactory, a European Consortium to Develop Technologies Needed to Advance Cyanobacteria as Chassis for Production of Chemicals and Fuels." *Algal Research* 41. https://www.sciencedirect.com/science/article/pii/S2211926418311275.

Liu, Haijun et al. 2019. "Phycobilisomes Harbor FNRL in Cyanobacteria." *mBio* 10: e00669-19. https://mbio.asm.org/content/10/2/e00669-19 (November 11, 2020).

Luimstra, Veerle M. et al. 2018. "Blue Light Reduces Photosynthetic Efficiency of Cyanobacteria through an Imbalance between Photosystems I and II." *Photosynthesis Research* 138(2): 177–89. https://link.springer.com/article/10.1007/s11120-018-0561-5 (March 31, 2020).

———. 2019. "Exploring the Low Photosynthetic Efficiency of Cyanobacteria in Blue Light Using a Mutant Lacking Phycobilisomes." *Photosynthesis Research* 141(3): 291–301. https://link.springer.com/article/10.1007/s11120-019-00630-z (March 31, 2020).

Ma, Weimin, Teruo Ogawa, Yungang Shen, and Hualing Mi. 2007. "Changes in Cyclic and Respiratory Electron

Transport by the Movement of Phycobilisomes in the Cyanobacterium Synechocystis Sp. Strain PCC 6803." *Biochimica et Biophysica Acta - Bioenergetics* 1767(6): 742–49. https://www.sciencedirect.com/science/article/pii/S0005272807000205 (March 31, 2020).

MacColl, Robert. 2004. "Allophycocyanin and Energy Transfer." *Biochimica et Biophysica Acta - Bioenergetics* 1657(2–3): 73–81. https://www.sciencedirect.com/science/article/pii/S000527280400091X (March 31, 2020).

Manodori, Annamaria, and Anastasios Melis. 1986. "Cyanobacterial Acclimation to Photosystem I or Photosystem II Light." *Plant Physiology* 82(1): 185–89. http://www.plantphysiol.org/content/82/1/185 (March 31, 2020).

McGee, Dónal et al. 2020. "Influence of Spectral Intensity and Quality of LED Lighting on Photoacclimation, Carbon Allocation and High-Value Pigments in Microalgae." *Photosynthesis Research* 143(1): 67–80. https://link.springer.com/article/10.1007/s11120-019-00686-x (March 31, 2020).

Moal, Gwenaëlle, and Bernard Lagoutte. 2012. "Photo-Induced Electron Transfer from Photosystem i to NADP+: Characterization and Tentative Simulation of the in Vivo Environment." *Biochimica et Biophysica Acta - Bioenergetics* 1817(9): 1635–45. https://linkinghub.elsevier.com/retrieve/pii/S0005272812001843 (March 31, 2020).

de Mooij, Tim et al. 2016. "Impact of Light Color on Photobioreactor Productivity." *Algal Research* 15: 32–42. https://www.sciencedirect.com/science/article/pii/S2211926416300261 (March 31, 2020).

Morel, André, and Annick Bricaud. 1981. "Theoretical Results Concerning Light Absorption in a Discrete Medium, and Application to Specific Absorption of Phytoplankton." *Deep Sea Research Part A, Oceanographic Research Papers* 28(11): 1375–93. https://www.sciencedirect.com/science/article/abs/pii/019801498190039X (March 31, 2020).

Münzner, Petra, and Jürgen Voigt. 1992. "Blue Light Regulation of Cell Division in Chlamydomonas Reinhardtii." *Plant Physiology* 99(4): 1370–75. http://www.plantphysiol.org/content/99/4/1370 (March 31, 2020).

Orr, Larry, and Govindjee. 2013. "Photosynthesis Web Resources." *Photosynthesis Research* 115(2–3): 179–214. https://link.springer.com/article/10.1007/s11120-013-9840-3 (March 28, 2020).

Porra, R. J., W. A. Thompson, and P. E. Kriedemann. 1989. "Determination of Accurate Extinction Coefficients and Simultaneous Equations for Assaying Chlorophylls a and b Extracted with Four Different Solvents: Verification

of the Concentration of Chlorophyll Standards by Atomic Absorption Spectroscopy." *BBA - Bioenergetics* 975(3): 384–94. https://www.sciencedirect.com/science/article/abs/pii/S0005272889803470 (March 31, 2020).

Rabe, A. E., and R. J. Benoit. 1962. "Mean Light Intensity—a Useful Concept in Correlating Growth Rates of Dense Cultures of Microalgae." *Biotechnology and Bioengineering* 4(4): 377–90. http://doi.wiley.com/10.1002/bit.260040404 (March 28, 2020).

Rakhimberdieva, M. G., V. A. Boichenko, N. V. Karapetyan, and I. N. Stadnichuk. 2001. "Interaction of Phycobilisomes with Photosystem II Dimers and Photosystem I Monomers and Trimers in the Cyanobacterium Spirulina Platensis." *Biochemistry* 40(51): 15780–88. https://pubs.acs.org/doi/10.1021/bi010009t (March 31, 2020).

Remelli, William, and Stefano Santabarbara. 2018. "Excitation and Emission Wavelength Dependence of Fluorescence Spectra in Whole Cells of the Cyanobacterium Synechocystis Sp. PPC6803: Influence on the Estimation of Photosystem II Maximal Quantum Efficiency." *Biochimica et Biophysica Acta - Bioenergetics* 1859(11): 1207–22. https://www.sciencedirect.com/science/article/pii/S000527281830642X (March 31, 2020).

Rögner, M., P. J. Nixon, and B. A. Diner. 1990. "Purification and Characterization of Photosystem I and Photosystem II Core Complexes from Wild-Type and Phycocyanin-Deficient Strains of the Cyanobacterium Synechocystis PCC 6803." *Journal of Biological Chemistry* 265(11): 6189–96. https://www.jbc.org/content/265/11/6189.long (March 31, 2020).

Simis, Stefan G.H., and Hanna M. Kauko. 2012. "In Vivo Mass-Specific Absorption Spectra of Phycobilipigments through Selective Bleaching." *Limnology and Oceanography: Methods* 10(4): 214–26. http://doi.wiley.com/10.4319/lom.2012.10.214 (March 31, 2020).

Singh, Abhay K. et al. 2009. "A Systems-Level Analysis of the Effects of Light Quality on the Metabolism of a Cyanobacterium." *Plant Physiology* 151(3): 1596–1608. http://www.plantphysiol.org/content/151/3/1596 (March 31, 2020).

Stirbet, Alexandrina, Dušan Lazár, George C. Papageorgiou, and Govindjee. 2019. "Chlorophyll a Fluorescence in Cyanobacteria: Relation to Photosynthesis." In *Cyanobacteria*, Elsevier, 79–130. https://linkinghub.elsevier.com/retrieve/pii/B9780128146675000052 (March 31, 2020).

Stramski, Dariusz, and André Morel. 1990. "Optical Properties of Photosynthetic Picoplankton in Different

Physiological States as Affected by Growth Irradiance." *Deep Sea Research Part A, Oceanographic Research Papers* 37(2): 245–66. https://www.sciencedirect.com/science/article/abs/pii/019801499090126G (March 31, 2020).

Takaichi, Shinichi, Takashi Maoka, and Kazumori Masamoto. 2001. "Myxoxanthophyll in Synechocystis Sp. PCC 6803 Is Myxol 2′-Dimethyl-Fucoside, (3R,2′S)-Myxol 2′-(2,4-Di-O-Methyl-α-l-Fucoside), Not Rhamnoside." *Plant and Cell Physiology* 42(7): 756–62. https://academic.oup.com/pcp/article/42/7/756/1863634 (March 31, 2020).

Thrane, Jan-Erik et al. 2015. "Spectrophotometric Analysis of Pigments: A Critical Assessment of a High-Throughput Method for Analysis of Algal Pigment Mixtures by Spectral Deconvolution" ed. Francois G. Schmitt. *PLOS ONE* 10(9): e0137645. https://dx.plos.org/10.1371/journal.pone.0137645 (March 31, 2020).

Tian, Lijin et al. 2011. "Site, Rate, and Mechanism of Photoprotective Quenching in Cyanobacteria." *Journal of the American Chemical Society* 133(45): 18304–11. https://pubs.acs.org/doi/10.1021/ja206414m (March 31, 2020).

Touloupakis, Eleftherios, Bernardo Cicchi, and Giuseppe Torzillo. 2015. "A Bioenergetic Assessment of Photosynthetic Growth of Synechocystis Sp. PCC 6803 in Continuous Cultures." *Biotechnology for Biofuels* 8(1): 133. http://www.biotechnologyforbiofuels.com/content/8/1/133 (March 31, 2020).

Tsunoyama, Yuichi et al. 2009. "Multiple Rieske Proteins Enable Short- and Long-Term Light Adaptation of Synechocystis Sp. PCC 6803." *Journal of Biological Chemistry* 284(41): 27875–83. https://www.jbc.org/content/284/41/27875 (March 31, 2020).

Tyystjärvi, Taina et al. 2002. "Action Spectrum of PsbA Gene Transcription Is Similar to That of Photoinhibition in Synechocystis Sp. PCC 6803." *FEBS Letters* 516(1–3): 167–71. https://febs.onlinelibrary.wiley.com/doi/10.1016/S0014-5793(02)02537-1 (March 31, 2020).

Umena, Yasufumi, Keisuke Kawakami, Jian Ren Shen, and Nobuo Kamiya. 2011. "Crystal Structure of Oxygen-Evolving Photosystem II at a Resolution of 1.9Å." *Nature* 473(7345): 55–60. https://www.nature.com/articles/nature09913 (March 31, 2020).

Vajravel, Sindhujaa et al. 2016. "β-Carotene Influences the Phycobilisome Antenna of Cyanobacterium Synechocystis Sp. PCC 6803." *Photosynthesis Research* 130(1–3): 403–15. https://link.springer.com/article/10.1007/s11120-016-0273-7 (March 31, 2020).

Warren, C. K., and B. C.L. Weedon. 1958. “804. Carotenoids and Related Compounds. Part VII. Synthesis of Canthaxanthin and Echinenone.” *Journal of the Chemical Society (Resumed)* (0): 3986–93. https://pubs.rsc.org/en/content/articlelanding/1958/jr/jr9580003986 (March 31, 2020).

Westermark, Stefanie, and Ralf Steuer. 2016. “Toward Multiscale Models of Cyanobacterial Growth: A Modular Approach.” *Frontiers in Bioengineering and Biotechnology* 4(DEC). https://www.frontiersin.org/articles/10.3389/fbioe.2016.00095/ (November 28, 2019).

von Wobeser, Eneas Aguirre et al. 2011. “Concerted Changes in Gene Expression and Cell Physiology of the Cyanobacterium Synechocystis Sp. Strain PCC 6803 during Transitions between Nitrogen and Light-Limited Growth.” *Plant Physiology* 155(3): 1445–57. http://www.plantphysiol.org/content/155/3/1445 (March 31, 2020).

Woźniak, Bogdan et al. 2003. “Modelling Light and Photosynthesis in the Marine Environment.” *Oceanologia* 45(2): 171–245.

Wright, SW, SW Jeffrey, and RFC Mantoura. 1997. Phytoplankton pigments in oceanography: guidelines to modern methods *Phytoplankton Pigments in Oceanography: Guidelines to Modern Methods*. UNESCO Publishing.

Yacobi, Y. Z., J. Köhler, F. Leunert, and A. Gitelson. 2015. “Phycocyanin-Specific Absorption Coefficient: Eliminating the Effect of Chlorophylls Absorption.” *Limnology and Oceanography: Methods* 13(4): e10015. http://doi.wiley.com/10.1002/lom3.10015 (March 31, 2020).

Zakar, Tomas et al. 2017. “Lipid and Carotenoid Cooperation-Driven Adaptation to Light and Temperature Stress in Synechocystis Sp. PCC6803.” *Biochimica et Biophysica Acta - Bioenergetics* 1858(5): 337–50. https://www.sciencedirect.com/science/article/pii/S0005272817300245 (March 31, 2020).

Zavřel, Tomáš et al. 2015. “Characterization of a Model Cyanobacterium *Synechocystis* Sp. PCC 6803 Autotrophic Growth in a Flat-Panel Photobioreactor.” *Engineering in Life Sciences* 15(1): 122–32. http://doi.wiley.com/10.1002/elsc.201300165 (March 31, 2020).

Zavřel, Tomáš, Petra Očenášová, and Jan Červený. 2017. “Phenotypic Characterization of Synechocystis Sp. PCC 6803 Substrains Reveals Differences in Sensitivity to Abiotic Stress” ed. Jon M. Jacobs. *PLOS ONE* 12(12): e0189130. https://dx.plos.org/10.1371/journal.pone.0189130 (March 31, 2020).

Zhang, Yao et al. 2017. “An Extended PROSPECT: Advance in the Leaf Optical Properties Model Separating Total

Chlorophylls into Chlorophyll a and B." *Scientific Reports* 7: 6429. https://www.nature.com/articles/s41598-017-06694-y (March 31, 2020).

Zhao, Wenfeng, Jie Xie, Xiuling Xu, and Jingquan Zhao. 2015. "State Transitions and Fluorescence Quenching in the Cyanobacterium Synechocystis PCC 6803 in Response to Changes in Light Quality and Intensity." *Journal of Photochemistry and Photobiology B: Biology* 142: 169–77. https://www.sciencedirect.com/science/article/abs/pii/S1011134414003741 (March 31, 2020).

Zlenko, Dmitry V. et al. 2019. "Role of the PB-Loop in ApcE and Phycobilisome Core Function in Cyanobacterium Synechocystis Sp. PCC 6803." *Biochimica et Biophysica Acta - Bioenergetics* 1860(2): 155–66. https://www.sciencedirect.com/science/article/pii/S0005272818301695 (March 31, 2020).

Pigment	Pigment description		
	Abs. peak λ_{max} (nm)	$a^*(\lambda_{max})$ ($m^2 \cdot$ mg pigment^{-1})	λ shift (nm)
- *Chlorophylls*			
Chlorophyll a	430	0.0213 [d]	+8
	662	0.0258 [d]	+18
- *Phycobiliproteins*			
Phycocyanin	612 [a]	0.0027	+12
Allophycocyanin	648 [b]	0.0030	+12
- *Carotenoids*			
β-carotene	454	0.0596 [e]	+12
Myxoxanthophyll	477	0.0495 [f]	+12
Zeaxanthin	452	0.0532 [g]	+12
Echinenone	458	0.0497 [h]	+12
3'-Hydroxyechinenone	496 [c]	0.0497	+12

Table 1. Characteristics of the main pigments used for the absorption-spectrum reconstruction. References shown next to a weight-specific absorption-coefficient indicate the value source, while those next to an in vitro peak wavelengths specify that the original works only contain the pigment distribution in relative units and thus, the corresponding coefficient had to be indirectly calculated as explained in the text. [a](Faccio et al. 2014), [b](MacColl 2004), [c](Chábera et al. 2011), [d](Lichtenthaler 1987), [e](Hiyama, Nishimura, and Chance 1969), [f](Hertzberg, Liaaen-Jensen, and Siegelman 1971), [g](Aasen and Jensen 1966), [h](Warren and Weedon 1958).

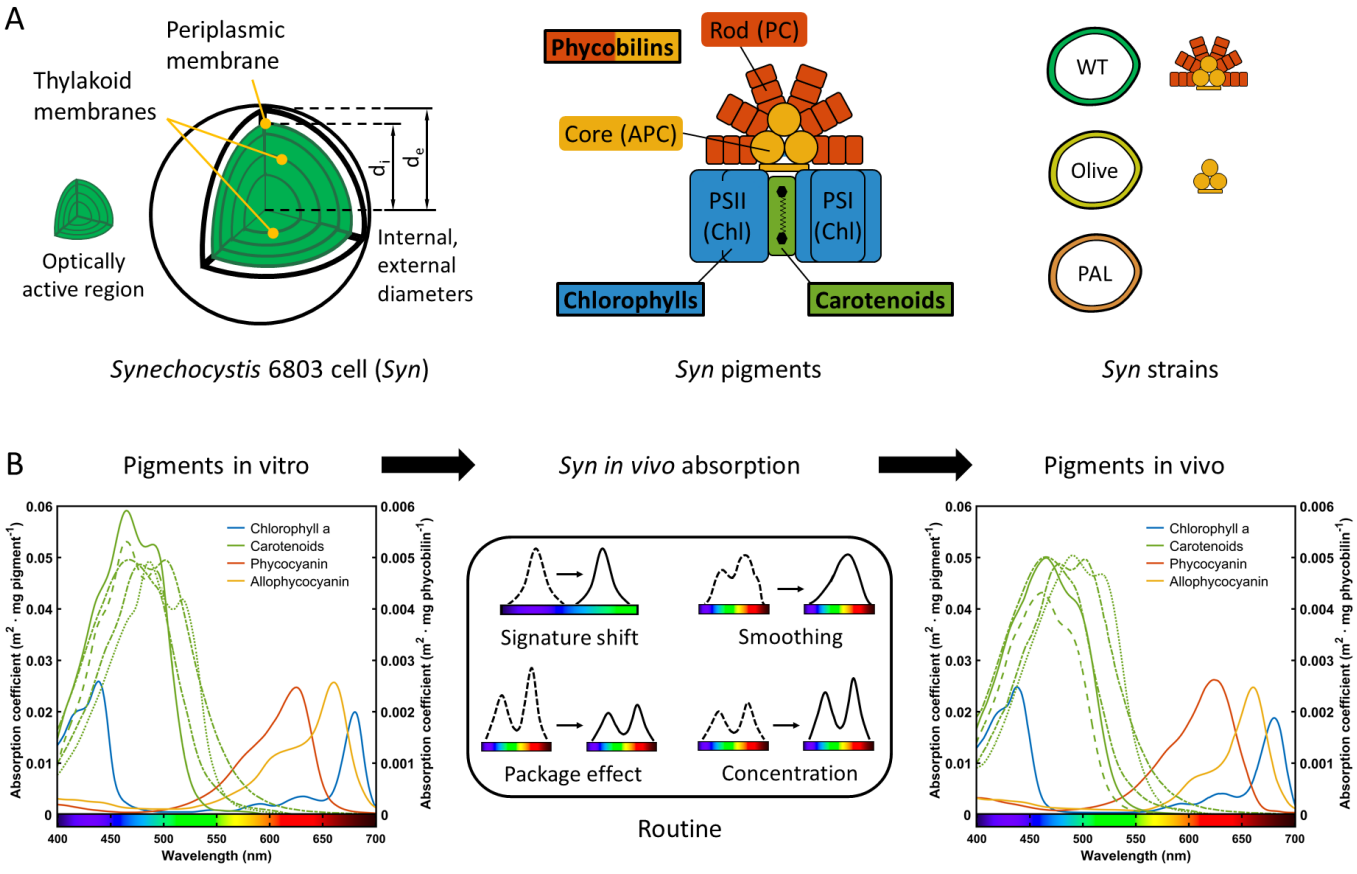

Figure 1. A, *Synechocystis* cell, its pigment location, pigment types and studied optical mutants. B, The in vitro absorption coefficients of *Synechocystis* pigments are the starting point for obtaining the in vivo signatures when the cell absorption spectrum is used as guideline.

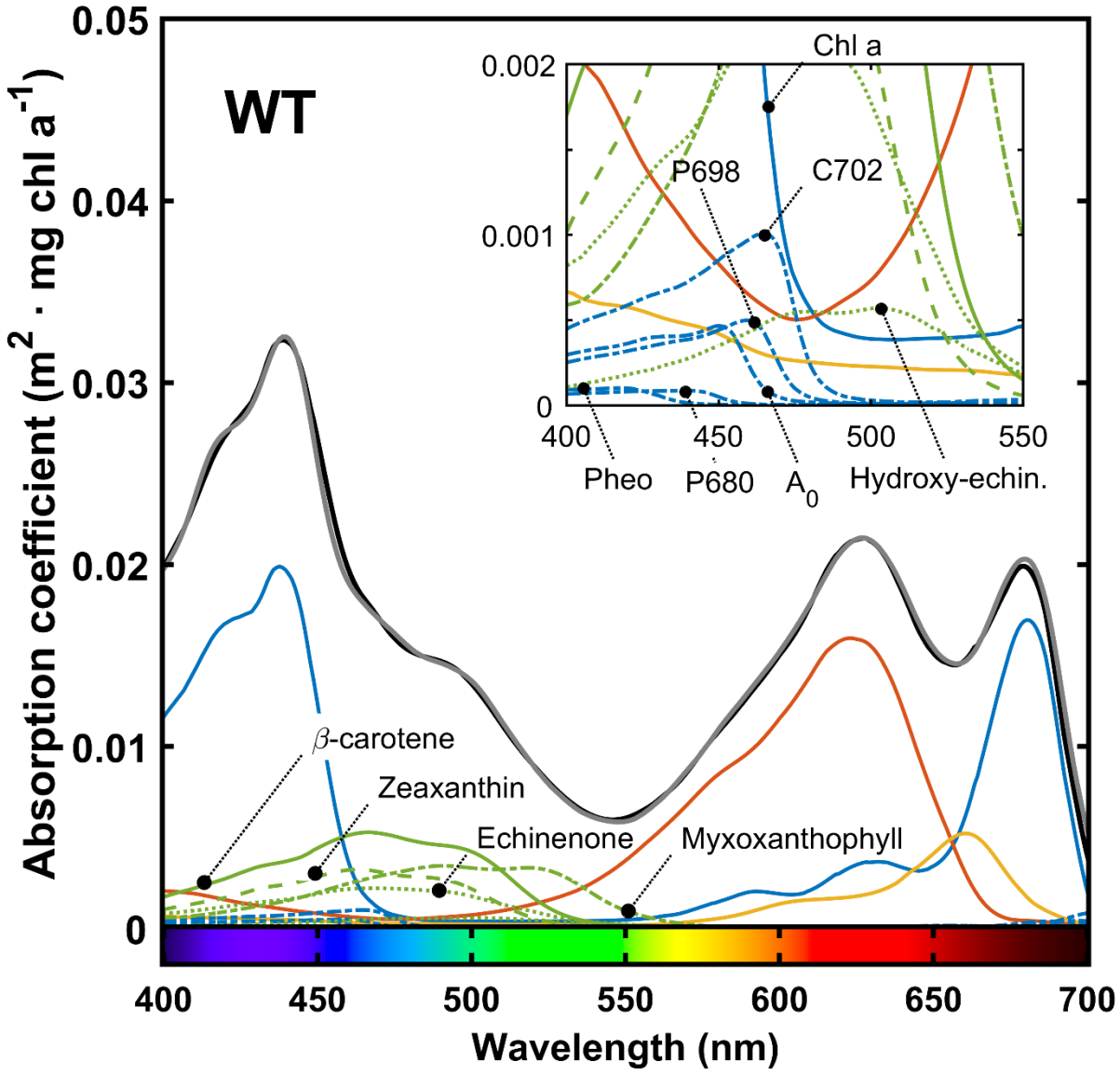

Figure 2. Reconstructed chlorophyll-specific absorption spectrum of *Synechocystis* WT cells acclimatized to 100 µmol photon · m^{-2} · s^{-1} of cool white LED light. The black signature corresponds to the reconstructed absorption, while the gray curve is the in vivo spectrum. Computed in vivo specific absorption coefficients for each pigment are also depicted: chlorophyll a (blue, solid) and related molecules (blue, dash-dotted), carotenoids (green) [*β*-carotene (solid), zeaxanthin (dashed), echinenone (dotted), 3' - hydroxyechinenone (dotted) and myxoxanthophyll (dash-dotted)], phycocyanin (red) and allophycocyanin (yellow). Inset plot shows for the shortest wavelengths the absorption spectrum of accessory PS molecules (blue, dash-dotted) [pheophytin (Pheo), PSII RC (P680), PSI primary

acceptor (A_0), PSI RC (P698) and the pool of red chlorophylls (C702)]. Each axis unit of the inset plot is identical to that of the main plot.

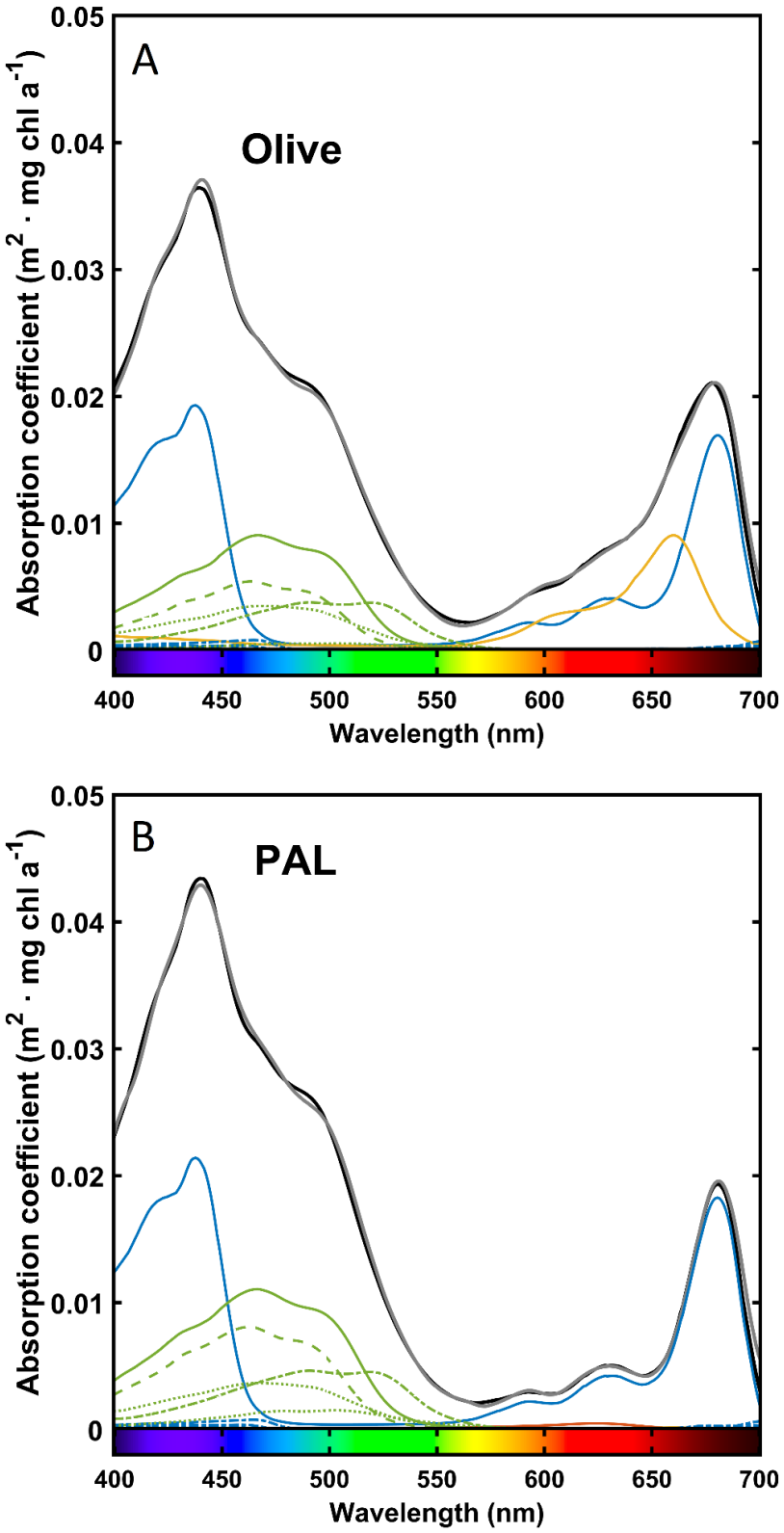

Figure 3. Reconstructed chlorophyll-specific absorption spectrum of *Synechocystis* Olive (A) and PAL (B) cells acclimatized to 100 µmol photon · m^{-2} · s^{-1} of cool white LED light. Same line colors and styles used for representing pigment chlorophyll-specific absorption coefficients as in Figure 2.

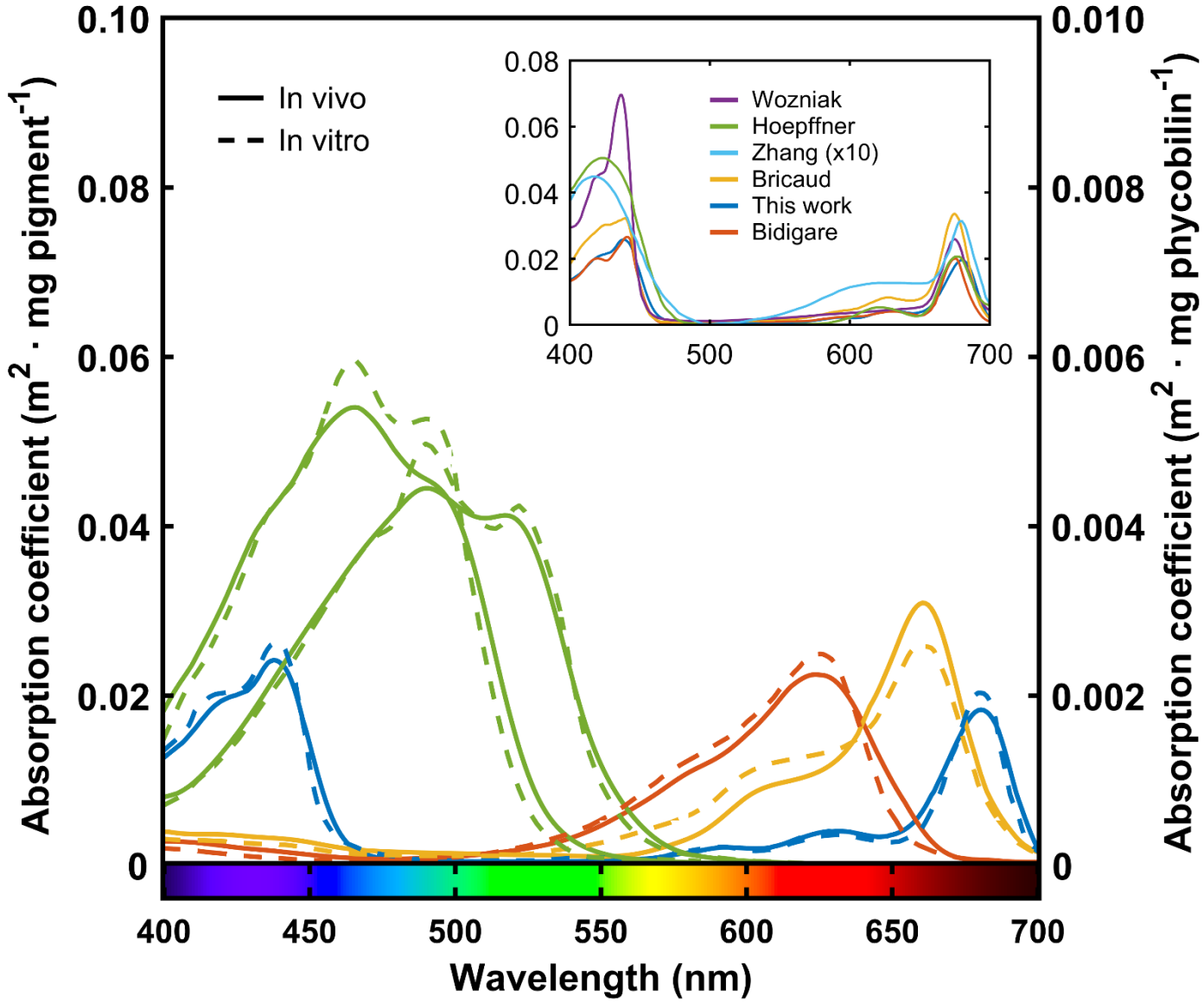

Figure 4. Comparison of the computed in vivo weight-specific absorption coefficients and the in vitro ones. For clarity, only β-carotene and myxoxanthophyll among all present carotenoids are shown. Left axis refers to chlorophyll a and carotenoid coefficients, the right axis to phycobilin ones. The inset plot displays the in vivo chlorophyll absorption spectrum proposed by different authors, whose referenced works can be found in the text. Each axis unit of the inset plot is identical to that of the main plot.

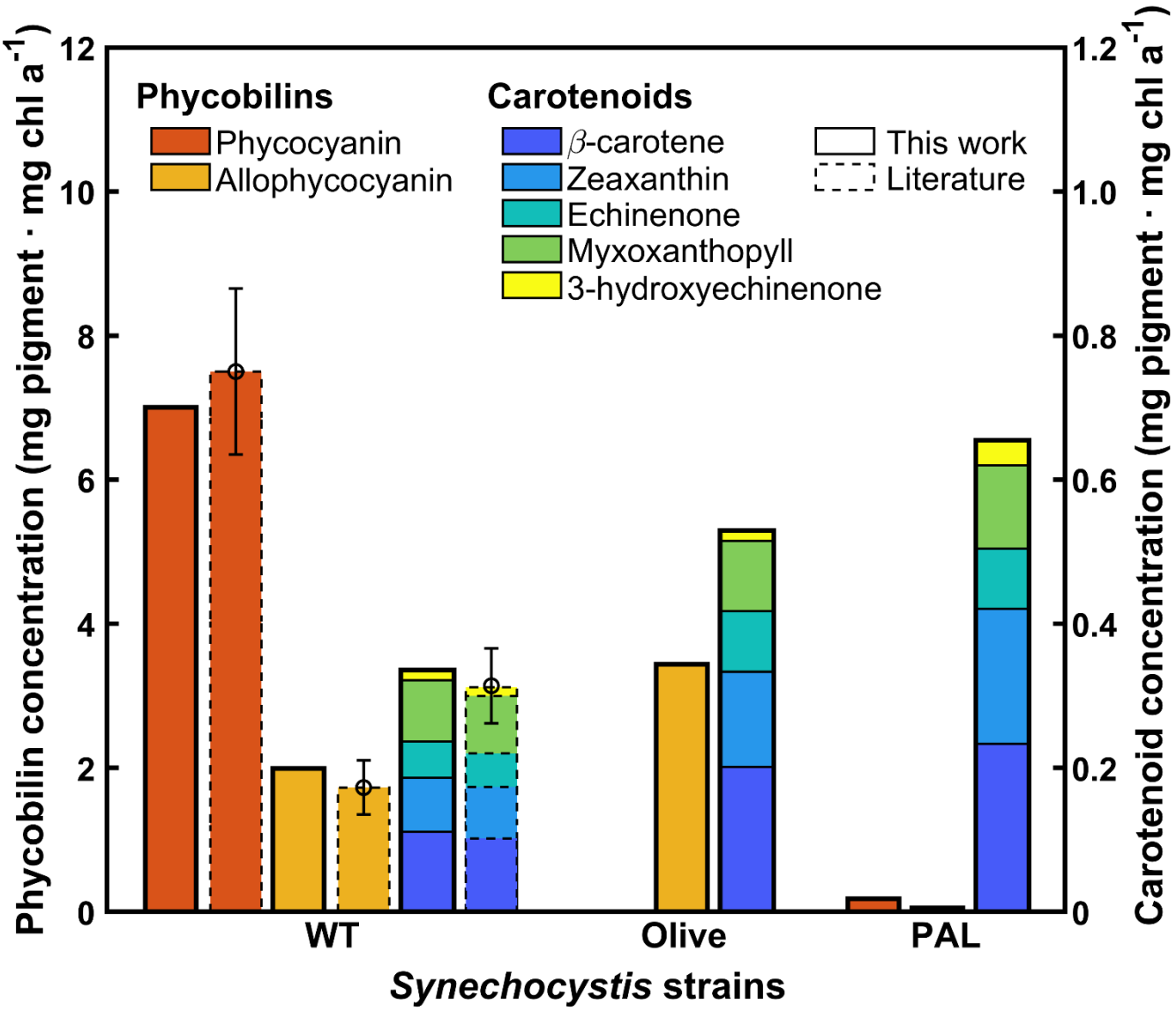

Figure 5. Calculated pigment concentration per chlorophyll-mass unit after in vivo absorption reconstruction for each studied *Synechocystis* strain. Literature works referenced in the text.

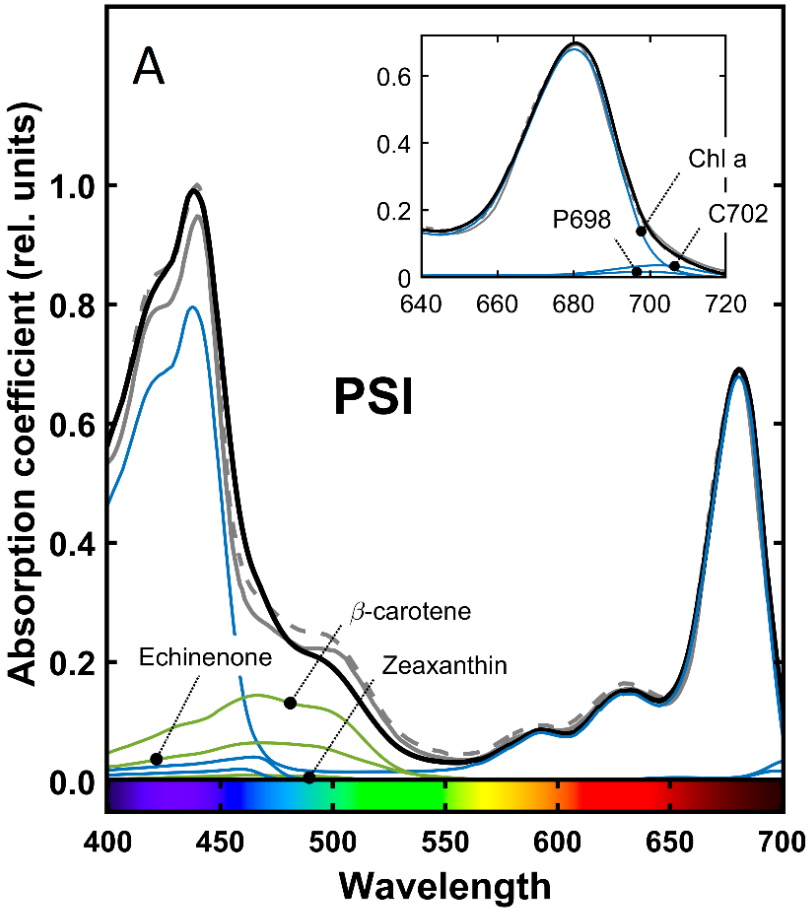
A
PSI
Absorption coefficient (rel. units)
Wavelength
Chl a
P698
C702
β-carotene
Echinenone
Zeaxanthin

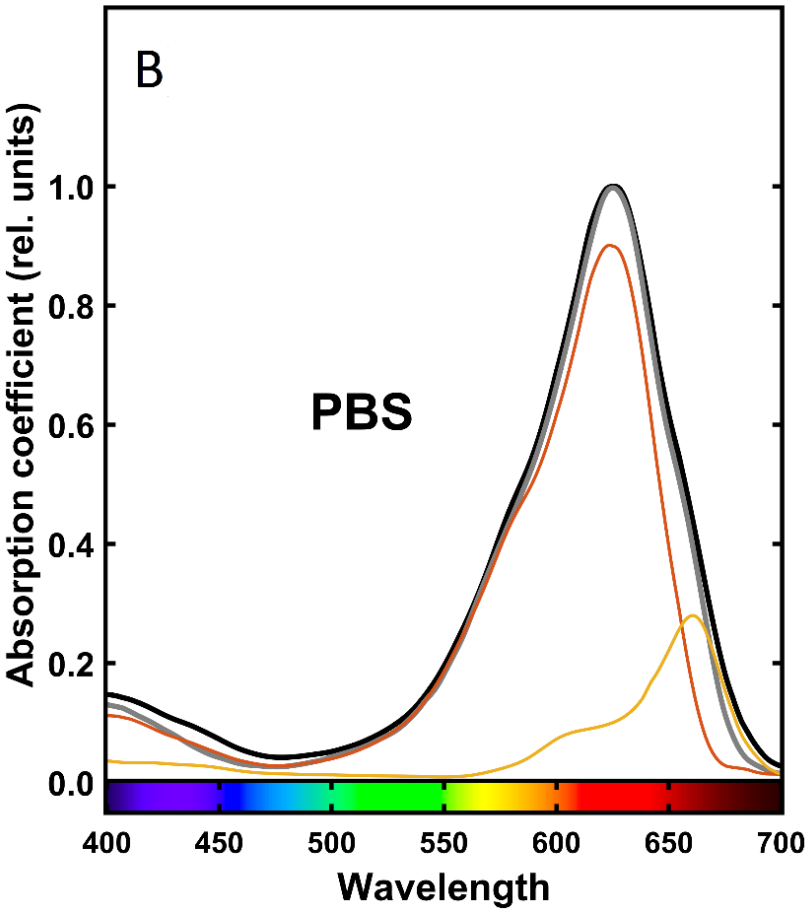
B
PBS
Absorption coefficient (rel. units)
Wavelength

Figure 6. A, The reconstructed absorption spectrum of PSI (black) in relative units is graphed as a combination of chlorophyll a, reaction center and red-shifted chlorophyll molecules (all in blue), and carotenoids (β-carotene, echinenone and zeaxanthin) following published mass proportions detailed in the main text. Prior-literature *Synechocystis* PSI absorption spectrum for monomeric (gray dashed) and trimeric (gray solid) states are also depicted. Inset plot displays the red-to-infrared waveband. Each axis unit of the inset plot is identical to that of the main plot. B, Reconstructed phycobilisome absorption spectrum (black) in relative units is graphed as a combination of phycocyanin (red) and allophycocyanin (yellow) molecules and compared with literature spectrum (gray). The sources for the experimental *Synechocystis* PSI and PBS absorption spectra are provided within the text.

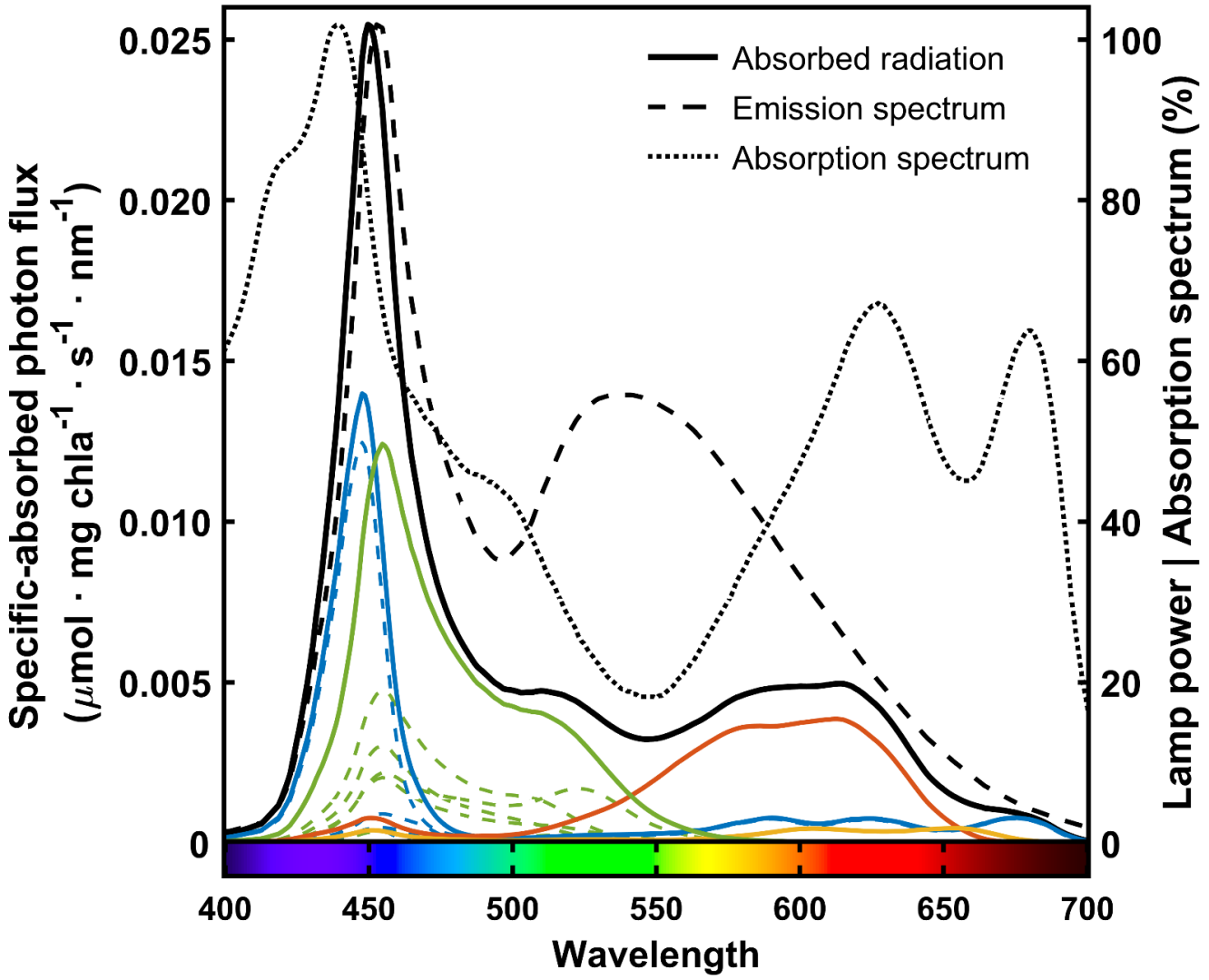

Figure 7. Chlorophyll-specific absorbed photon flux (black solid) by *Synechocystis* cells long-term exposed to 100 µmol photon · m^{-2} · s^{-1} emitted by a cool white LED. The photon flux arises from the sum of the light absorbed by different pigment groups (same colors used as in previous figures). For chlorophyll-related molecules (blue) and carotenoids (green), all the class-belonging chromophores are also drawn (dashed). Lamp emission spectrum (black dashed) and cell absorption (black dotted) have been normalized with respect to their corresponding maxima for clarity.

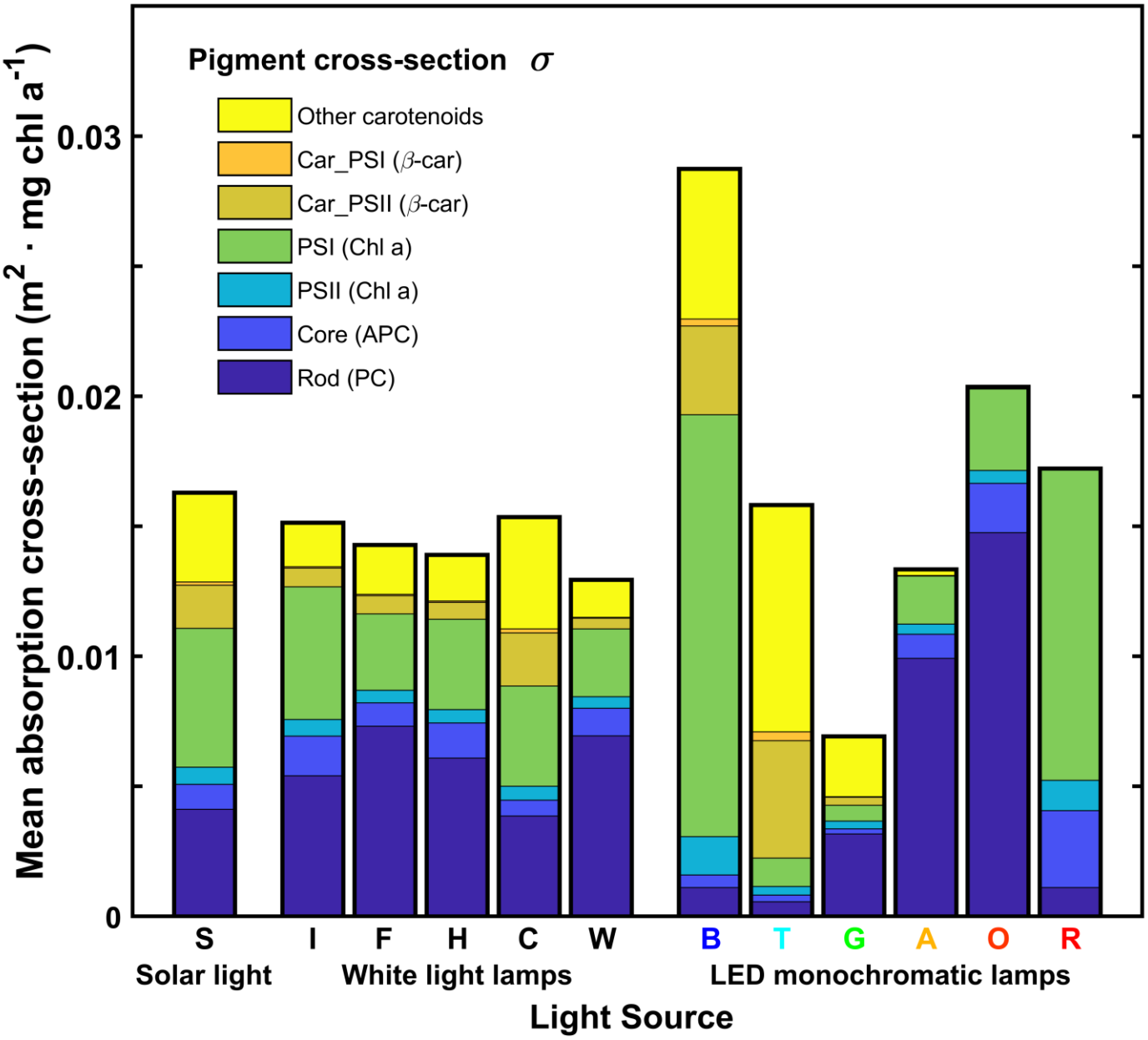

Figure 8. Mean chlorophyll-specific absorption cross-section of individual pigments for *Synechocystis* cells acclimatized to a total intensity of 100 µmol photon · m^{-2} · s^{-1}. Altogether, these build up the mean cell cross-section. Pigment absorption is partitioned into the main light harvesting structures present in the cells (including their chromophores): PBS rod (PC), PBS core (APC), PSII (Chl. a), PSI (Chl. a), light harvesting carotenoids of PSII (*β*-carotene), of PSI (*β*-carotene) and the rest of carotenoids. The emission spectra of the used light sources are shown in the same order in Supplemental Figure S5.

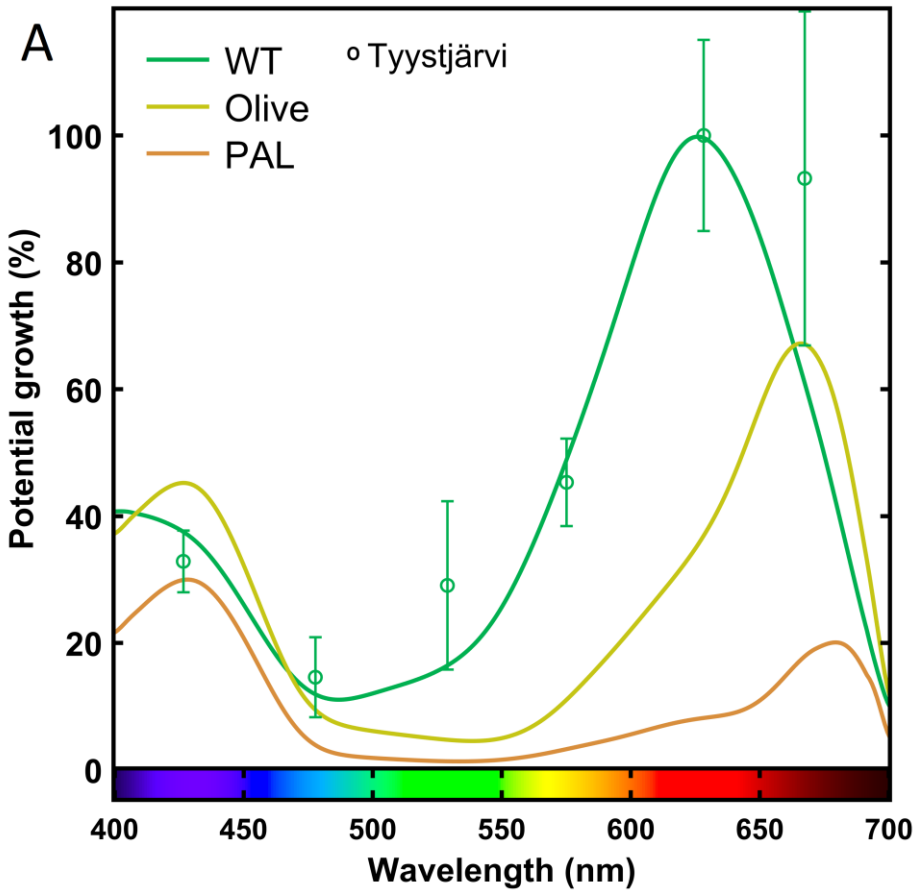
A
WT
Olive
PAL
Tyystjärvi
Potential growth (%)
0
20
40
60
80
100
400
450
500
550
600
650
700
Wavelength (nm)

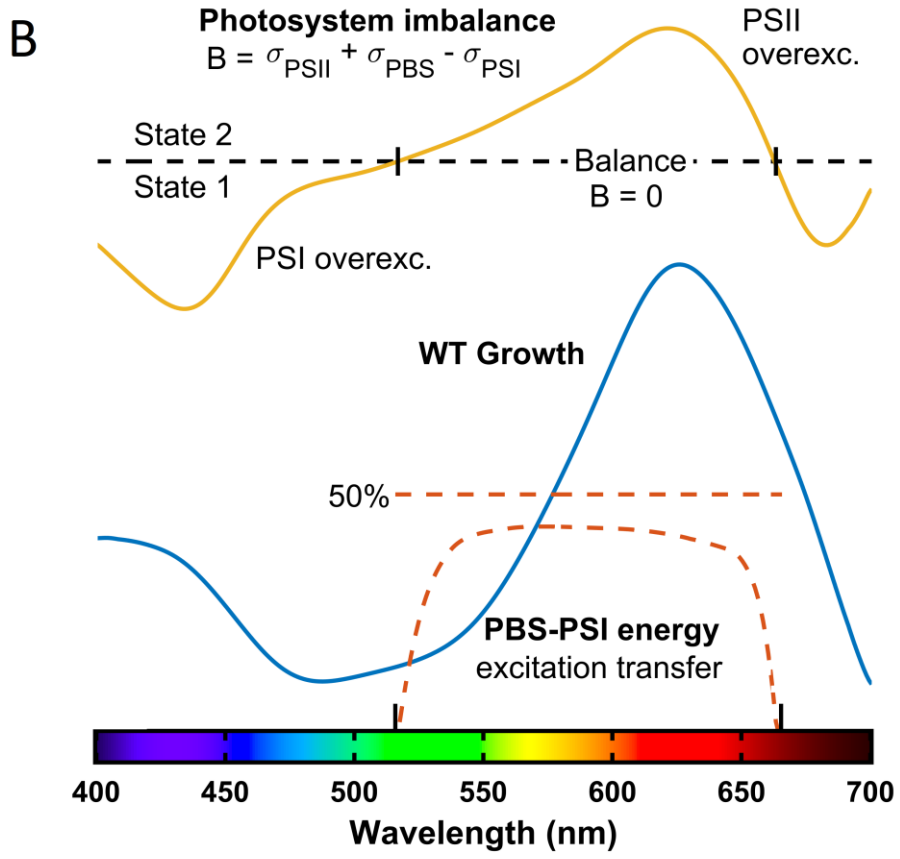
B
Photosystem imbalance
B = σPSII + σPBS - σPSI
PSII overexc.
State 2
State 1
Balance
B = 0
PSI overexc.
WT Growth
50%
PBS-PSI energy
excitation transfer
400
450
500
550
600
650
700
Wavelength (nm)

Figure 9. A, The growth potential of each strain under limited light is shown. Each strain growth is normalized to the WT maximal one. Experimental data for WT are also displayed (reference in text). B, The energy-balance driving force of state-transitions is outlined. The initial photosystem excitation imbalance for WT, represented as the sum of PSII and PBS absorption cross-sections minus the PSI one is depicted (yellow). The corresponding potential growth (blue) and the required PBS-PSI transfer for energy re-equilibration (red) are also plotted.

Supplementary Material

Package-effect calculation

In the following, the package-effect derivation will be described. Pigment coefficients inside living cells are always lower than those measured in dispersed homogeneous solutions, also referred to as unpacked coefficients. This absorption reduction is set by the dimensionless factor $Q^*_a(\lambda)$ representing the package effect:

$$Q_a^*(\lambda) = \frac{a^*(\lambda)}{a_{sol}^*(\lambda)} \tag{S1}$$

where a^* is the true absorption coefficient and a_{sol} the one of the ideally dispersed pigment solution. In order to reconstruct the true in vivo cell absorption spectrum from in vitro coefficients and in this way calculate all pigment concentrations, the package effect has to be determined. Such magnitude can be estimated by means of the theoretical framework proposed by Morel et al. (Morel and Bricaud, 1981):

$$Q_a^*(\rho') = \frac{3}{2}\frac{Q_a^*(\rho')}{\rho'} \tag{S2}$$

Hence, the dimensionless factor ρ', which rules the discreteness of absorption, must be previously calculated. To do so, homogeneity and sphericity of the cells have to be assumed and in this regard most of *Synechocystis* photo-active pigments are located in the plasma and thylakoid membranes. In addition, the latter layers are structured as spherical membranes within the cell (Fig. 1A), similarly to "matryoshka dolls" following an intra-laminar arrangement (Liberton *et al.*, 2006). Therefore, the homogeneity assumption seems plausible in this strain. Additionally, prior works have already shown satisfactory results when assuming a spherical approximation for spheroidal cells (Bricaud, Bédhomme and Morel, 1988; Nelson and Prézelin, 1990). The experimental absorption efficiency, knowing the measured in vivo absorption spectrum, is given at each wavelength λ by:

$$Q_a^*(\lambda) = \frac{2}{3}a^*(\lambda)c_i d_i \tag{S3}$$

being c_i the intracellular chlorophyll concentration and d_i the cell internal diameter. This is valid for the case of equally-sized particles of diameter d_i. However, at the culture scale it is common to find a population of cells with different diameters. This is the so called polydispersion and its effect is taken into account through the size distribution function $F(d)$. Mathematically, $F(d)$ is treated as a weight function, so the efficiency factor will be weighted as follows (Bricaud and Morel, 1986):

$$\bar{Q}_a(\rho') = \frac{\int_0^\infty Q_a^*(\rho')F(\rho')\rho'^2 d\rho'}{\int_0^\infty F(\rho')\rho'^2 d\rho'} \tag{S4}$$

Then the anomalous diffraction approximation, which was described by Van de Hulst (van de Hulst, 1957) and is a particular case of the Mie-Lorentz theory, will be leveraged. The approximation is based on the next assumptions: the size of the particles is one order of magnitude larger than the wavelength, hence the parameter α, defined in Equation (S7), is greater than 10 and the particles are weakly absorbing and therefore the imaginary part of the refractive index n' is close to zero. Thanks to these assumptions, a simple analytic function of Q_a is available. Once the efficiency magnitude has been computed via Equations (S3) and (S4), the relationship (S5) can be solved for ρ' at each wavelength:

$$Q_a(\rho') = 1 + 2\frac{e^{-\rho'}}{\rho'} + 2\frac{e^{-\rho'}-1}{\rho'^2} \tag{S5}$$

Note that ρ' and λ are linked via Equations (S6) and (S7). Afterwards, the imaginary part of the refractive index n' can be determined, taking into consideration following relationships:

$$n' = \frac{\rho'}{4\alpha} \quad \text{(S6)}$$

$$\lambda = \frac{\pi d_i}{\alpha} \quad \text{(S7)}$$

doing so, we will able to check out that at any wavelength λ, n' is close to zero as initially postulated. Finally, the package effect can be computed through the Equation (S2).

In order to assess the package effect, several cell properties are necessary: the internal diameter d_i, the cell-chlorophyll content, the cell size distribution of each strain and the true absorption spectrum. To obtain the first variable, the external cell diameter d_e can be first measured and the periplasmic space subtracted, whose depth approximately accounts for 0.05 µm as micrograph pictures of this strain indicate (Liberton *et al.*, 2006). The cell size distribution measured in (Moal and Lagoutte, 2012) was assumed for all strains.

Bricaud, A., Bédhomme, A. louise and Morel, A. (1988) 'Optical properties of diverse phytoplanktonic species: Experimental results and theoretical interpretation', *Journal of Plankton Research*, 10(5), pp. 851–873. doi: 10.1093/plankt/10.5.851.

Bricaud, A. and Morel, A. (1986) 'Light attenuation and scattering by phytoplanktonic cells: a theoretical modeling', *Applied Optics*. The Optical Society, 25(4), p. 571. doi: 10.1364/ao.25.000571.

van de Hulst, H. C. (1957) *Light scattering by small particles*. John Wiley. doi: 10.1002/qj.49708436025.

Liberton, M. *et al.* (2006) 'Ultrastructure of the membrane systems in the unicellular cyanobacterium Synechocystis sp. strain PCC 6803', *Protoplasma*. Springer, 227(2–4), pp. 129–138. doi: 10.1007/s00709-006-0145-7.

Moal, G. and Lagoutte, B. (2012) 'Photo-induced electron transfer from photosystem i to NADP+: Characterization and tentative simulation of the in vivo environment', *Biochimica et Biophysica Acta - Bioenergetics*. Elsevier, 1817(9), pp. 1635–1645. doi: 10.1016/j.bbabio.2012.05.015.

Morel, A. and Bricaud, A. (1981) 'Theoretical results concerning light absorption in a discrete medium, and application to specific absorption of phytoplankton', *Deep Sea Research Part A, Oceanographic Research Papers*. Elsevier, 28(11), pp. 1375–1393. doi: 10.1016/0198-0149(81)90039-X.

Nelson, N. and Prézelin, B. (1990) 'Chromatic light effects and physiological modeling of absorption properties of Heterocapsa pygmaea (= Glenodinium sp.)', *Marine Ecology Progress Series*. Inter-Research Science Center, 63, pp. 37–46. doi: 10.3354/meps063037.

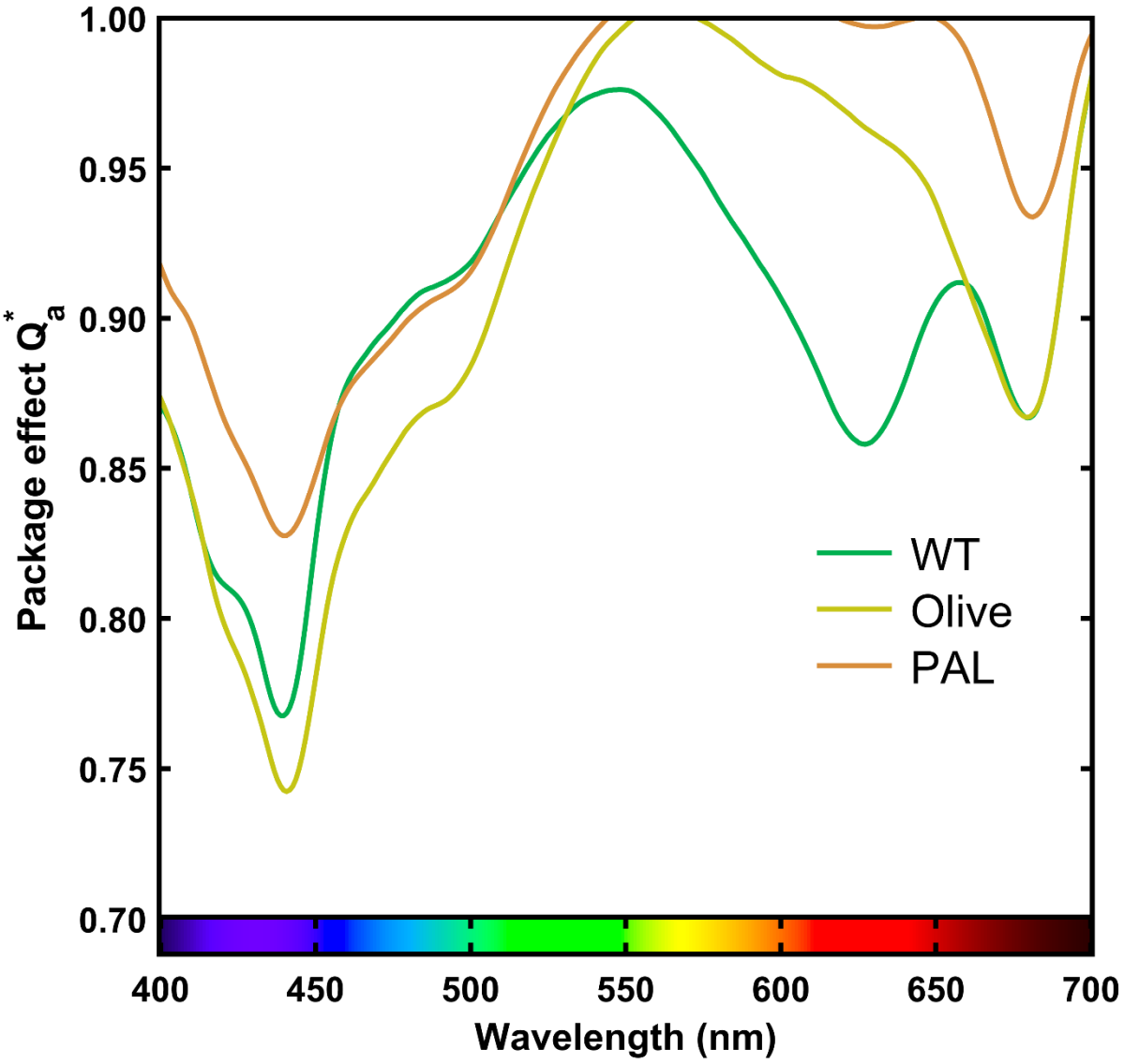

Figure S1. Computed package effect factor $Q_a^*(\lambda)$ for *Synechocystis* optical strains.

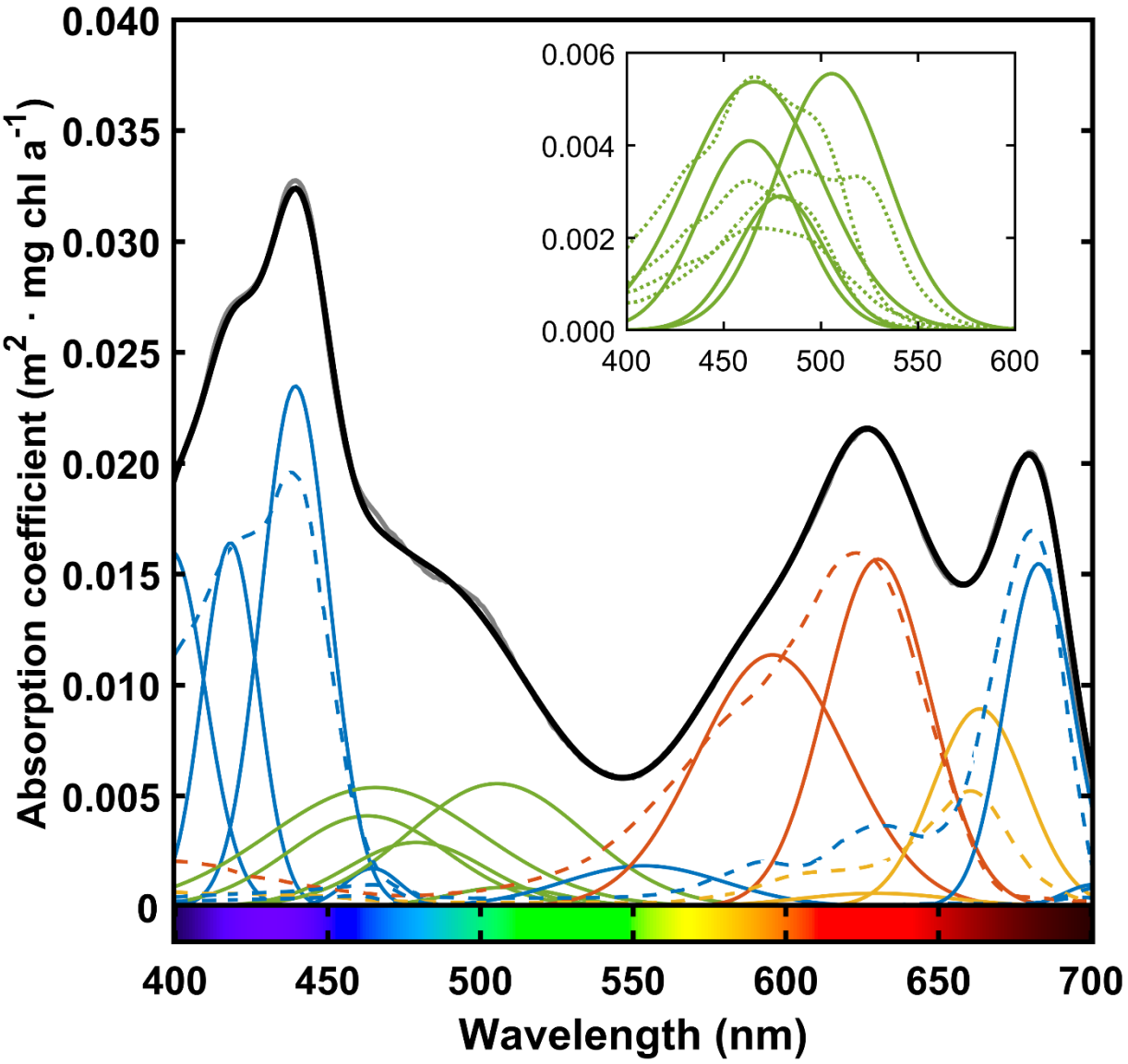

Figure S2. Reconstruction of WT absorption spectrum through Gaussian distributions: in this work assumed in vivo pigment signatures (dashed) are shown together with estimated Gaussian-reconstruction curves (solid). For clarity, the carotenoids β-carotene, zeaxanthin, echinenone and myxoxanthophyll have been depicted in the inset plot. Each axis unit of the inset plot is identical to that of the main plot. Colors represent same light harvesting compounds as in Figure 2.

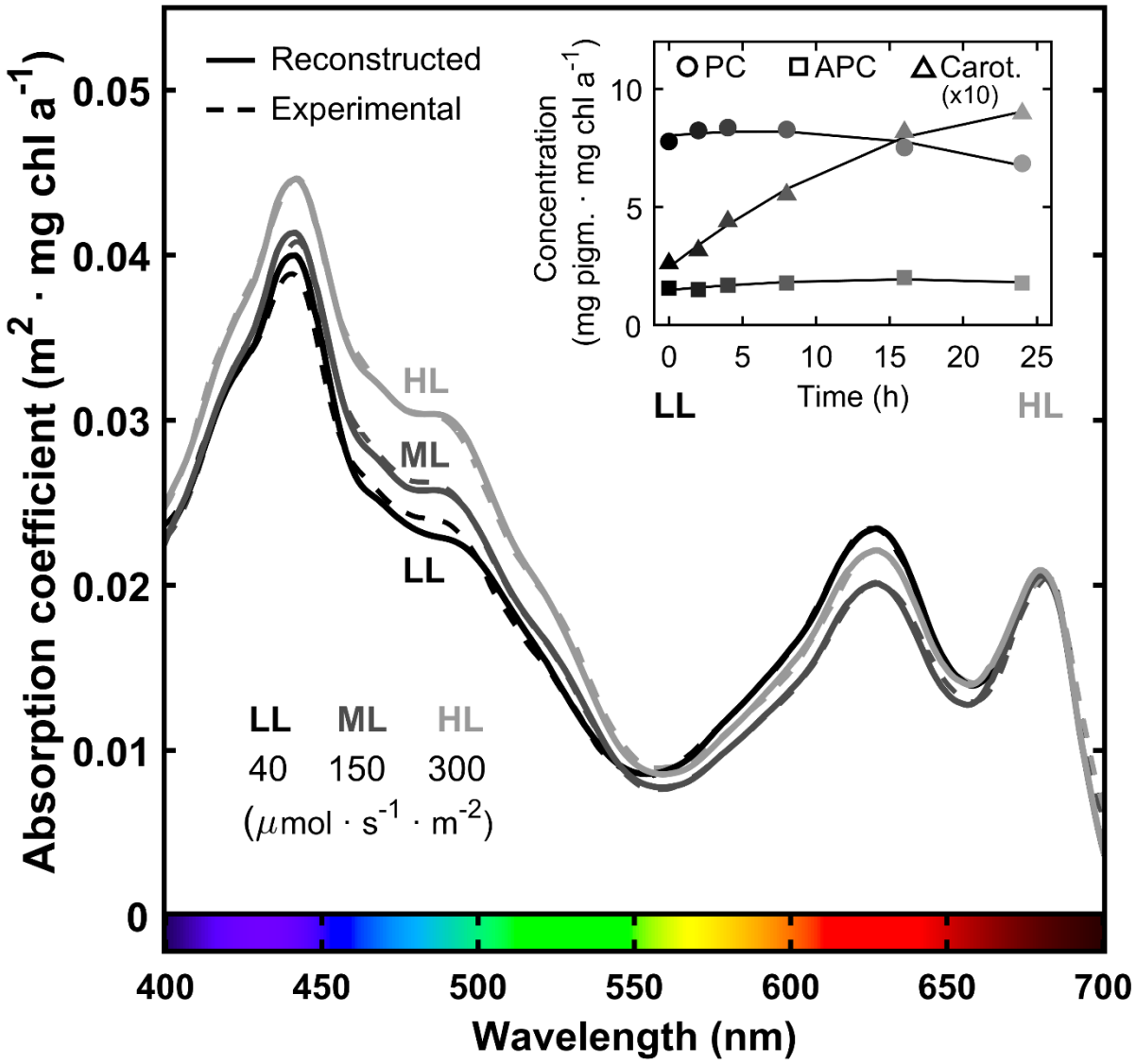

Figure S3. Chlorophyll-specific absorption coefficient of *Synechocystis* WT cells exposed to low (LL), medium (ML) and high-light (HL). The solid lines correspond to the reconstructed absorption, while the dashed ones are the spectra from the experimental work, referenced in the text. Darker colors indicate lower irradiance. Inset plot shows pigment time evolution in a LL-to-HL experiment.

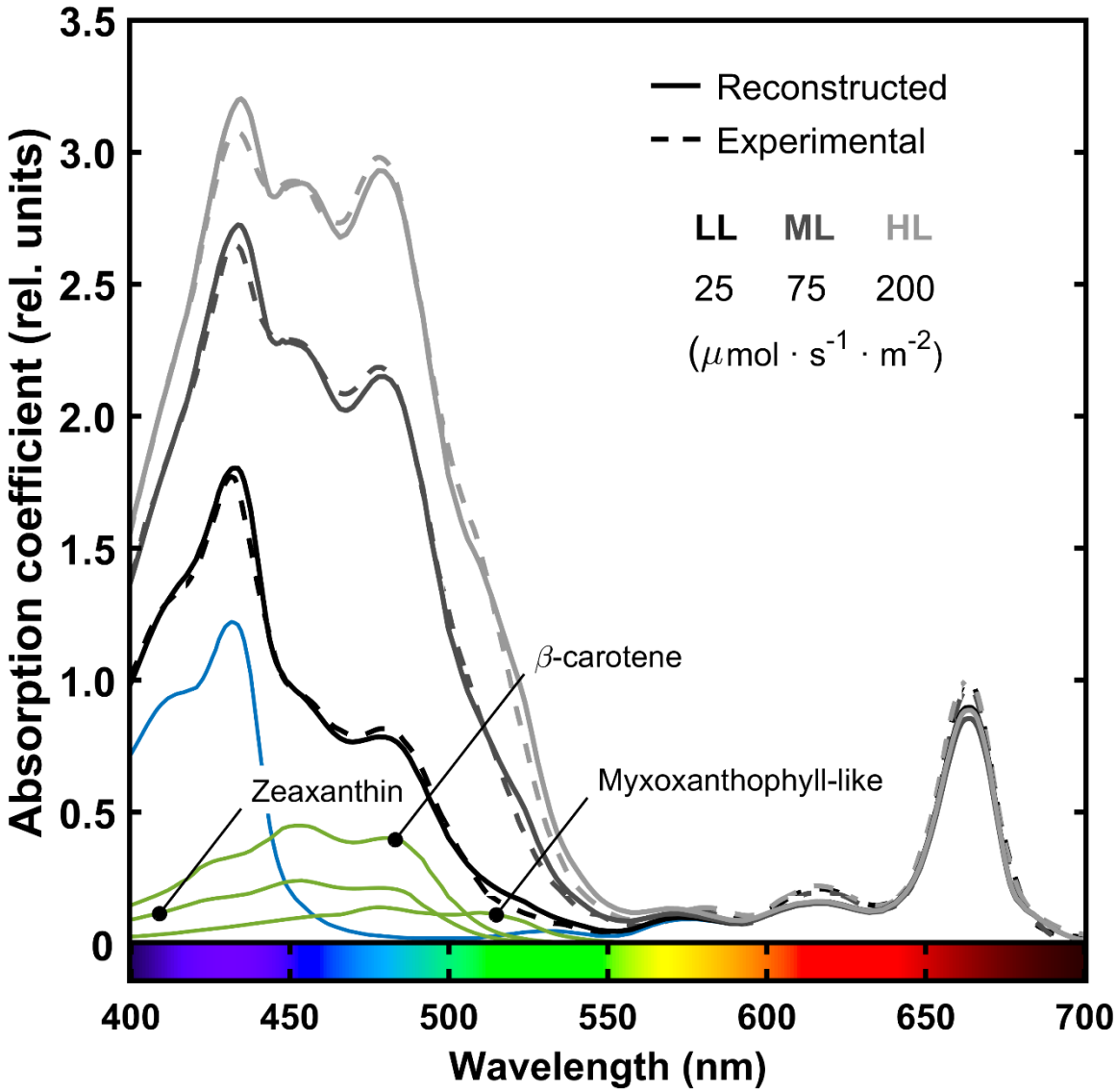

Figure S4. The absorption coefficients of cell extracts of *Synechococcus* OS' in relative units are displayed. Reconstructed spectra (solid) and experimental ones (dashed) are plotted. Different cultures were acclimated to different light intensities as indicated by the line colors.

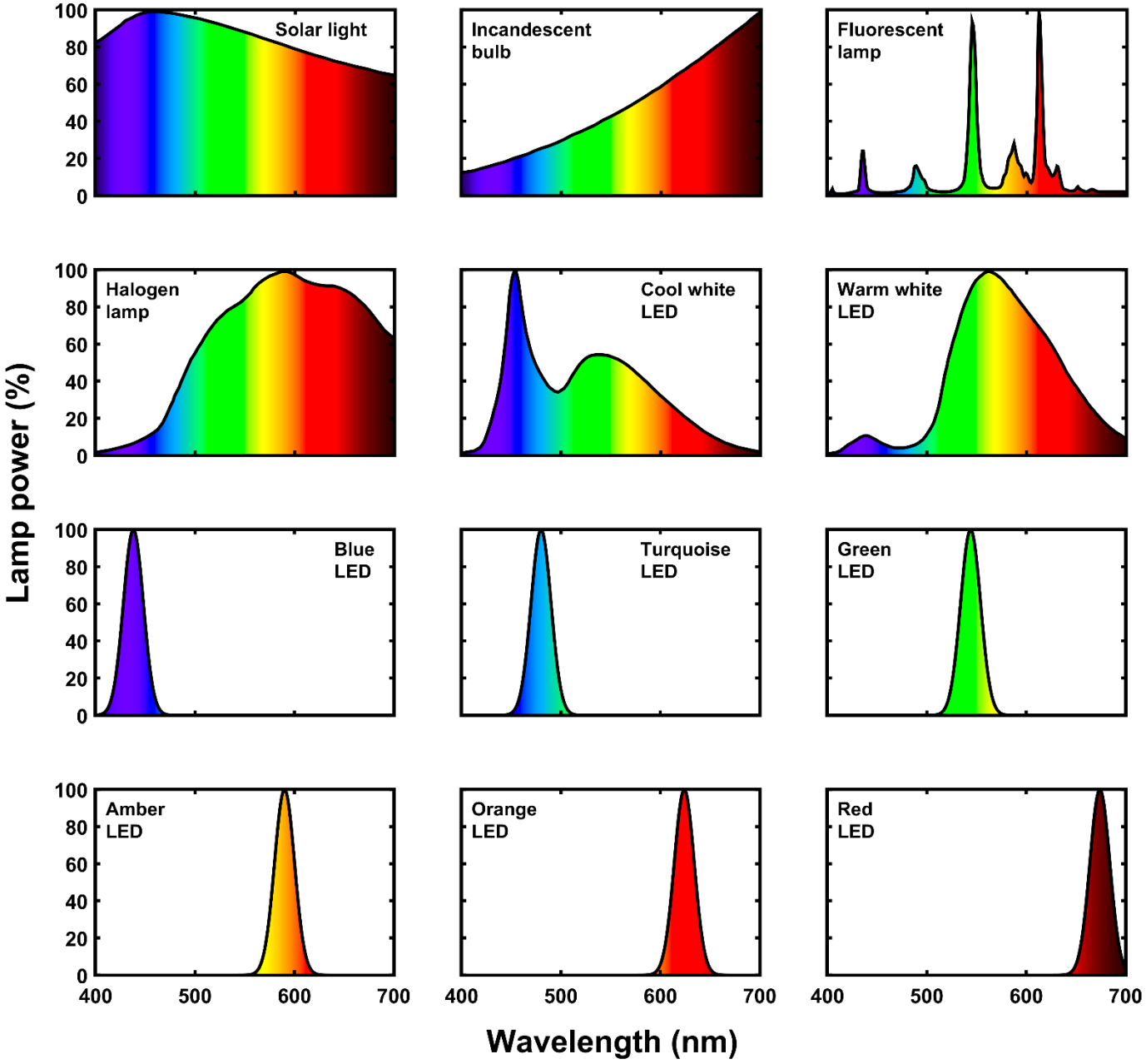

Figure S5. The photon-flux distribution of common light sources are shown in relative units. The flux distribution is depicted with the color of the corresponding wavelengths. These are the flux distributions used for estimating absorbed photon flux and cross-sections displayed in Figure 7, Figure 8 and Supplemental Figure S6.

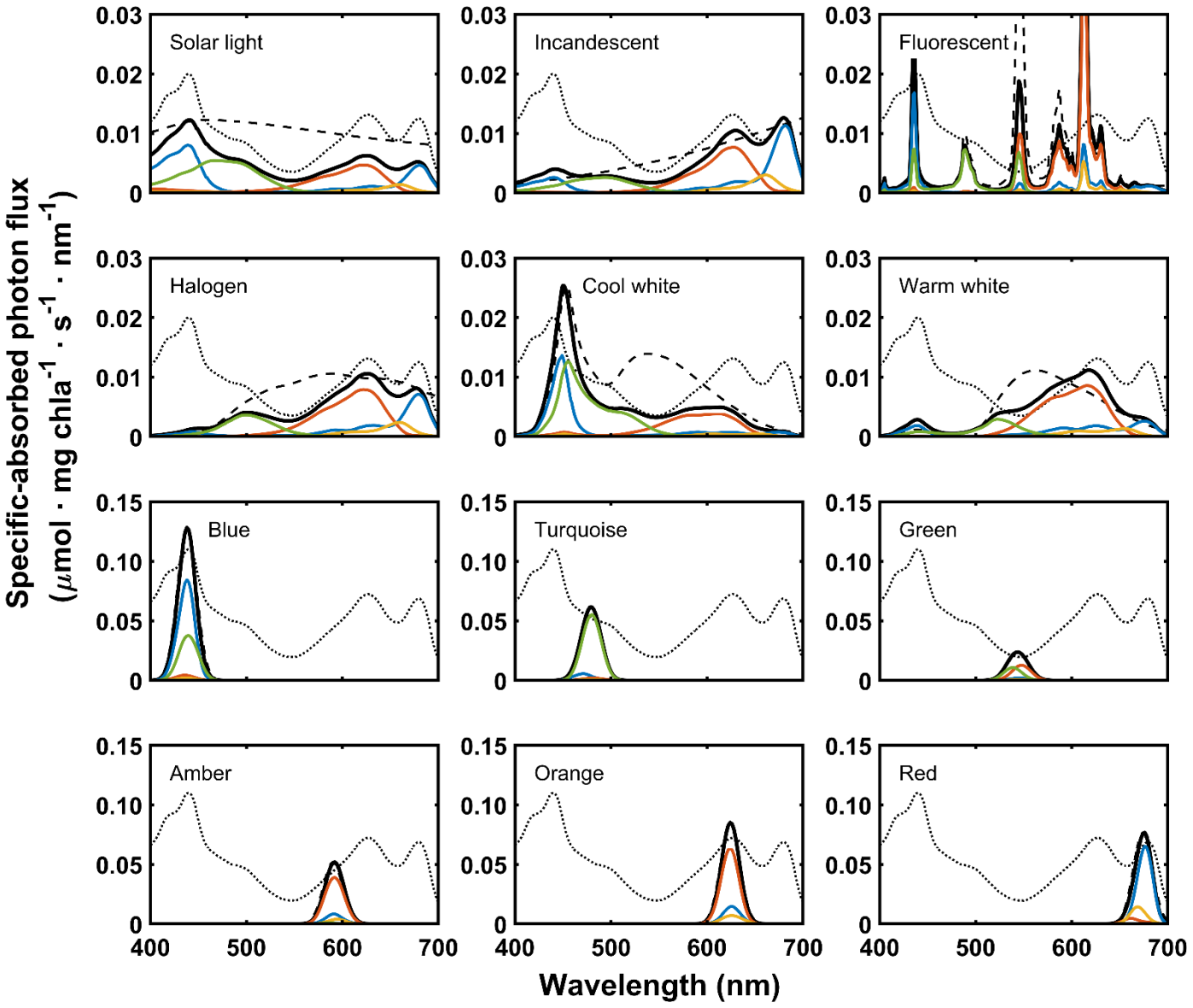

Figure S6. Chlorophyll-specific absorbed photon flux (black solid) by *Synechocystis* WT cells grown under 100 µmol photon · m^{-2} · s^{-1} of cool white LED and momentarily exposed to different light sources. Same colors used for each chromophore type (chlorophylls, carotenoids, phycocyanin and allophycocyanin) as shown in previous figures. The lamp emission spectrum (dashed) has been normalized with respect to the maximal absorbed photon flux. Cell absorption (dotted) has also been included in arbitrary units for clarity.